A&A 487, 33–46 (2008)
DOI: 10.1051/0004-6361:200809620

Astronomy & Astrophysics

Optical analysis of the poor clusters Abell 610, Abell 725, and Abell 796, containing diffuse radio sources⋆

W. Boschin[1,2], R. Barrena[3], M. Girardi[2,4], and M. Spolaor[2,5]

[1] Fundación Galileo Galilei – INAF, Rambla José Ana Fernández Perez 7, 38712 Breña Baja (San Antonio), Canary Islands, Spain
e-mail: boschin@tng.iac.es
[2] Dipartimento di Astronomia, Università degli Studi di Trieste, via Tiepolo 11, 34143 Trieste, Italy
[3] Instituto de Astrofisica de Canarias, C/Via Lactea s/n, 38205 La Laguna, Tenerife, Canary Islands, Spain
[4] INAF - Osservatorio Astronomico di Trieste, via Tiepolo 11, 34143 Trieste, Italy
[5] Centre for Astrophysics & Supercomputing, Swinburne University, Hawthorn, VIC 3122, Australia

Received 20 February 2008 / Accepted 14 April 2008

ABSTRACT

Aims. We study the dynamical status of the poor, low X-ray luminous galaxy clusters Abell 610, Abell 725, and Abell 796 (at z = 0.1, 0.09, and 0.16, respectively), containing diffuse radio sources (relic, relic, and possible halo, respectively).
Methods. Our analysis is based on new spectroscopic data obtained at the William Herschel Telescope for 158 galaxies, new photometry obtained at the Isaac Newton Telescope with the addition of data recovered from the Data Release 5 of the Sloan Digital Sky Survey. We use statistical tools to select 57, 36, and 26 cluster members and to analyze the kinematics of cluster galaxies, as well as to study the 2D cluster structure.
Results. The low values we compute for the global line-of-sight velocity dispersion of galaxies (σ_V = 420−700 km s^{-1}) confirm that these clusters are low-mass clusters. Abell 610 shows a lot of evidence of substructure. It seems to be formed by two structures separated by ∼700 km s^{-1} in the cluster rest-frame, having comparable σ_V ∼ 200 km s^{-1} and likely causing a velocity gradient. The velocity of the brightest cluster member (BCMI; a bright radio source) is very close to the mean velocity of the higher velocity structure. A third small, low-velocity group hosts the second brightest cluster member (BCMII). The analysis of the 2D galaxy distribution shows a bimodal distribution in the core elongated in the SE–NW direction and likely associated to BCMI and BCMII groups. Abell 725 and Abell 796, which are less sampled, show marginal evidence of substructure in the velocity space. They are elongated in the 2D galaxy distribution. For both Abell 610 and Abell 725 we shortly discuss the possible connection with the hosted diffuse radio relic.
Conclusions. Our results show that relic radio sources are likely connected with merger events, but are not limited to massive clusters. About the possible halo source in Abell 796, there is some evidence of a merger event in this non-massive cluster, but a pointed radio observation is necessary to confirm this halo.

Key words. galaxies: clusters: general – galaxies: clusters: individual: Abell 610 – galaxies: clusters: individual: Abell 725 – galaxies: clusters: individual: Abell 796 – galaxies: distances and redshifts – cosmology: observations

1. Introduction

Clusters of galaxies are not recognized as simple relaxed structures, but rather as evolving via merging processes in a hierarchical fashion from poor groups to rich clusters. A recent aspect of these investigations is the possible connection of cluster mergers with the presence of extended, diffuse radio sources: halos and relics. These radio sources are large (up to ∼1 h_{70}^{-1} Mpc), amorphous cluster sources of uncertain origin and generally steep radio spectra (Hanisch 1982; see also Giovannini & Feretti 2002, for a more recent review). They are rare sources that appear to be associated with very rich clusters that have undergone recent mergers. Therefore, it has been suggested by various authors that cluster halos/relics are related to recent merger activity (e.g., Tribble 1993; Burns et al. 1994; Feretti 1999).

The synchrotron radio emission of halos and relics demonstrates the existence of large scale cluster magnetic fields, of the order of 0.1−1 μG, and of widespread relativistic particles of energy density 10^{-14}−10^{-13} erg cm^{-3}. The difficulty in explaining radio halos/relics arises from the combination of their large size and the short synchrotron lifetime of relativistic electrons. The expected diffusion velocity of the electron population is of the order of the Alfven speed (∼100 km s^{-1}), making it difficult for the electrons to diffuse over a megaparsec-scale region within their radiative lifetime. Therefore, one needs a mechanism by which the relativistic electron population can be transported over large distances in a short time, or a mechanism by which the local electron population is reaccelerated and the local magnetic fields are amplified over an extended region. The cluster-cluster merger can potentially supply both mechanisms (e.g., Giovannini et al. 1993; Burns et al. 1994; Röttgering et al. 1994; see also Feretti et al. 2002; Sarazin 2002, for reviews). However, the question is still debated since the diffuse radio sources are quite uncommon and only recently have we been able to study these phenomena on the basis of sufficient statistics (few dozen clusters up to z ∼ 0.3, e.g., Giovannini et al. 1999; see also Giovannini & Feretti 2002; Feretti 2005).

Growing evidence of the connection between diffuse radio emission and cluster merging is based on X-ray data (e.g., Böhringer & Schuecker 2002; Buote 2002). Studies based on

⋆ Tables 1, 4, 5 are only available in electronic form at http://www.aanda.org

a large number of clusters have found a significant relation between the radio and the X-ray surface brightness (Govoni et al. 2001a,b) and between the presence of radio halos/relics and irregular and bimodal X-ray surface brightness distribution (Schuecker et al. 2001).

Optical data are a powerful way to investigate the presence and the dynamics of cluster mergers, too (e.g., Girardi & Biviano 2002). The spatial and kinematical analysis of member galaxies allow us to detect and measure the amount of substructure, to identify and analyze possible pre-merging clumps or merger remnants. This optical information is complementary to X-ray information since galaxies and intracluster medium react on different timescales during a merger (see, e.g., numerical simulations by Roettiger et al. 1997). Unfortunately, to date optical data are lacking or are poorly exploited to investigate the phenomenon of diffuse radio sources. The sparse literature contains a few individual clusters (e.g., Barrena et al. 2002; Mercurio et al. 2003; Maurogordato et al. 2008).

In this context, we are conducting an intensive observational and data analysis program to study the internal dynamics of radio clusters by using member galaxies. Clusters already analyzed are: Abell 2219 (Boschin et al. 2004); Abell 2744 (Boschin et al. 2006); Abell 697 (Girardi et al. 2006); Abell 773 (Barrena et al. 2007a); Abell 115 (Barrena et al. 2007b). These are all massive clusters and, indeed, to date analyzed clusters containing a radio halo or a relic source have a large gravitational mass (larger than $0.7 \times 10^{15}\ h_{70}^{-1}\ M_{\odot}$ within $2\ h_{70}^{-1}$ Mpc; see Giovannini & Feretti 2002). From the theoretical point of view, a large mass is an expected property in radio clusters since the energy available to accelerate relativistic particles in a merger scales as $\sim M^2$, as discussed by Buote (2001).

In this paper, we report our results about three poor Abell clusters: Abell 610, Abell 725, and Abell 796 (hereafter A610, A725, and A796) having Abell richness (i.e., the number of galaxies within 1 Abell radius and magnitude between m_3 and $m_3 + 2$; see Abell et al. 1989) of 46, 36, and 56 galaxies respectively. These clusters contain a radio relic or a (possible) radio halo. In particular, A610 exhibits a relic source confirmed by pointed observations (Giovannini & Feretti 2000); A725 presents a relic source well visible in survey data (Kempner & Sarazin 2001); and A796 possibly hosts a halo source visible in survey data (Kempner & Sarazin 2001) which needs to be confirmed. To date, no measure of internal velocity dispersion and/or X-ray temperature have been reported in the literature. We have recently carried out spectroscopic observations with the William Herschel Telescope giving new redshift data for 158 galaxies in the field of these clusters, as well as photometric observations at the Isaac Newton Telescope for A725. We recover additional photometric and spectroscopic information from the Data Release 5 of the Sloan Digital Sky Survey (SDSS DR5).

The paper is organized as follows. We present the new optical data in Sect. 2. We present the relevant analyses and conclusions in Sects. 3–5 for A610, A725, and A796, respectively. We summarize and discuss our results in Sect. 6.

Unless otherwise stated, we give errors at the 68% confidence level (hereafter c.l.). Throughout the paper, we assume a flat cosmology with $\Omega_{\rm m} = 0.3$, $\Omega_{\Lambda} = 0.7$ and $H_0 = 70\ h_{70}$ km s^{-1} Mpc^{-1}. For this cosmological model, 1′ corresponds to 108, 102, and 163 h_{70}^{-1} kpc at the A610, A725, and A796 redshift.

2. Data sample

2.1. Spectroscopy

We carried out multi-object spectroscopic observations of A610, A725, and A796 in November 2004 and January 2005. We used AF2/WYFFOS, the multi-object, wide-field, fiber spectrograph working at the prime focus of the 4.2 m William Herschel Telescope (WHT, Island of La Palma, Spain). This spectrograph is equipped with optical fibers each of 1.6 arcsec diameter. We used the grism R300B in combination with the 2-chip EEV 4 K × 4 K pixel mosaic (pixel size 13.5 μm) working in binning 2 × 2. In the case of A610 and A725, we acquired two exposures of 1800 s for two fiber configurations, in the case of A796 we acquired three exposures of 1800 s for two fiber configurations. We performed wavelength calibration with the helium lamp. Reduction of spectroscopic data was carried out with the IRAF package[1].

We determined radial velocities with the cross-correlation technique (Tonry & Davis 1979) implemented in the RVSAO package (developed at the Smithsonian Astrophysical Observatory Telescope Data Center). Each spectrum was correlated against six templates for a variety of galaxy spectral types: E, S0, Sa, Sb, Sc and Ir (Kennicutt 1992). The template producing the highest value of $\mathcal{R}$, i.e., the parameter given by RVSAO and related to the signal-to-noise of the correlation peak, was chosen. Moreover, all the spectra and their best correlation functions were examined visually to verify the redshift determination. In one case (galaxy ID 127 of A610, see Table 1), we took the EMSAO redshift as a reliable estimate of the redshift. We obtained redshifts for 62, 51, 45 galaxies for A610, A725, A796.

For ten galaxies we obtained two redshift determinations of similar quality. This allows us to obtain a more rigorous estimate for the redshift errors since the nominal errors as given by the cross-correlation are known to be smaller than the true errors (e.g., Malumuth et al. 1992; Bardelli et al. 1994; Ellingson & Yee 1994; Quintana et al. 2000). For these ten galaxies we fit the first determination vs. the second one by using a straight line and considering errors in both coordinates (e.g., Press et al. 1992). The fitted line agrees with the one-to-one relation, but, when using the nominal cross-correlation errors, the small value of the χ^2 probability indicates a poor fit, suggesting the errors are underestimated. Only when nominal errors are multiplied by a factor of ∼1.3 can the observed scatter be justified. We therefore assume hereafter that true errors are larger than nominal cross-correlation errors by a factor 1.3. For the ten galaxies we used the weighted mean of the two redshift determinations and the corresponding error.

For A610 and A796 we add galaxies with spectroscopic and/or photometric data found in the SDSS DR5. For A610, we find 147 galaxies within a radius of 30′ from the cluster center given by Abell et al. (1989). This radius is about the double of that sampled by our data and well larger than the virial radius of the cluster (see Sect. 3.1), and thus will be useful to study the cluster periphery, too. Out of 147 SDSS galaxies, 44 are in common with our WHT galaxies. We fit SDSS redshift determination vs. our determination finding that the fitted line well agrees with the one-to-one relation. Again, the small value of the χ^2 probability indicates a poor fit, suggesting the errors are

[1] IRAF is distributed by the National Optical Astronomy Observatories, which are operated by the Association of Universities for Research in Astronomy, Inc., under cooperative agreement with the National Science Foundation.

underestimated, but we prefer to not apply any correction since the measurements come from two different sources. We combine WHT and SDSS data using the weighted mean of the two redshift determinations and the corresponding error. Our final spectroscopic catalog consists of 165 galaxies. As for A796, we find 72 SDSS galaxies – out of which there are 18 in common with our WHT galaxies – and compile a final spectroscopic catalog of 99 galaxies.

2.2. Photometry

Our photometric observations were carried out with the Wide Field Camera (WFC), mounted at the prime focus of the 2.5 m Isaac Newton Telescope (INT, Island of La Palma, Spain). We observed A725 in December 2004 in photometric conditions with a seeing of about 1.8″ in R_H (Harris) band and 2.5″ in B_H.

The WFC consists of a four-CCD mosaic covering a 33′×33′ field of view, with only a 20% marginally vignetted area. We took 9 exposures of 720 s in B_H and another 13 exposures of 360 s in R_H filters (a total of 6480 s and 4680 s in the two bands, respectively). We developed a dithering pattern to build a "supersky" frame that was used to correct our images for fringing patterns (Gullixson 1992). In addition, the dithering helped us to clean cosmic rays and avoid gaps between the CCDs in the final images. The complete reduction process (including flat fielding, bias subtraction, and bad-column elimination) yielded a final coadded image where the variation of the sky was lower than 1.0% within a region of 13′ radius from the center of the cluster.

In order to match the photometry of several filters, a good astrometric solution is needed. The astrometry has to take into account the field distortions present in the WFC full frame. Using IRAF tasks and taking as a reference the USNO B1.0 catalog, we were able to find an accurate astrometric solution (rms ∼ 0.5″) across the full frame.

We performed the photometric calibration with Landolt standard fields observed in December 2007 using the 80 cm telescope at Teide Observatory. We finally identified galaxies in our B_H and R_H images and measured their magnitudes with the SExtractor package (Bertin & Arnouts 1996) and the AUTOMAG procedure. In a few cases (e.g., objects close to very bright and saturated stars) the standard SExtractor photometric procedure failed. In these cases, by performing an isophotal analysis (task *bmodel* in IRAF) we eliminate the bright objects. Then, we reran SExtractor to estimate the magnitudes of faint targets close to bright stars.

We transformed all Harris magnitudes into the Johnson-Cousins system (Johnson & Morgan 1953; Cousins 1976). We used $B = B_H + 0.13$ and $R = R_H$ as derived from the Harris filter characterization (http://www.ast.cam.ac.uk/~wfcsur/technical/photom/colours/) and assuming a $B - V \sim 1.0$ for E-type galaxies (Poggianti 1997). As a final step, we estimated and corrected the galactic extinction $A_B \sim 0.23$, $A_R \sim 0.14$ and $E(B-V) = 0.05$ from Burstein & Heiles's (1982) reddening maps.

The photometric sample of galaxies in the field of A725 is complete down to $B = 22.5$ (24.4) and $R = 20.6$ (22.1) for $S/N = 5$ (3) within a square region of 33′ × 33′ centered on RA = $09^h00^m50^s$ and Dec = +62°39′00″ (J2000), and with a void of 11′ × 11′ in the NW of the field. As for the spectroscopic sample, it is ∼25% complete down to $R = 17.5$ in the whole field and ∼45% complete down to $R = 17.5$ within 1 Mpc from the cluster center.

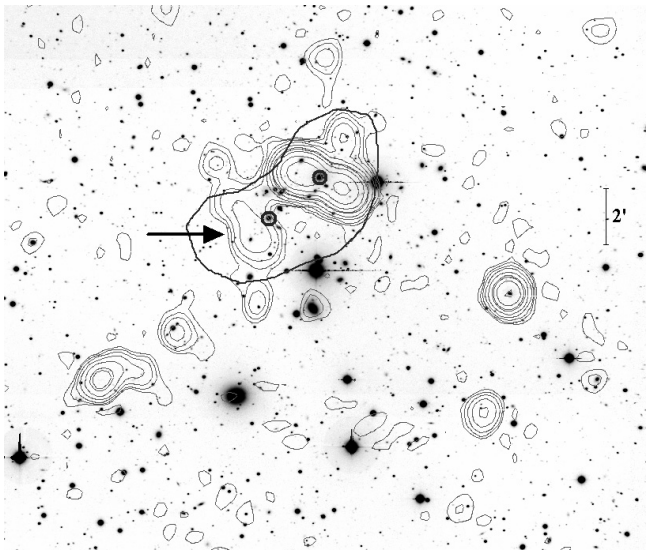

Fig. 1. *R*-band image of A610 (data taken with the WFC camera of the INT) with, superimposed, the contour levels of a VLA radio image at 20 cm (thin contours; Giovannini & Feretti 2000). To avoid confusion, only one isodensity contour (thick contour) of the spatial distribution of the likely cluster members (see text) is shown. Two thick circles highlight the positions of the two brightest cluster members. The arrow shows the position of the radio relic. *North is at the top and east to the left.*

For A610 and A796, we use public photometric data from the SDSS DR5. In particular, we use r', i', z' magnitudes, already corrected for the Galactic extinction and consider galaxies within a radius of 30′ from the cluster center given by Abell et al. (1989). In the case of A610, our spectroscopic sample is ∼40% complete down to $r' = 17.5$ within 1 Mpc from the cluster center. As for A796, our spectroscopic sample is ∼20% complete down to $r' = 19$ within 1 Mpc from the cluster center.

3. Abell 610

A610 is a poor Abell cluster (Abell richness class = 0; Abell et al. 1989) located in the background of the rich nearby cluster ZwCl 0752.9+2833 (at $z = 0.015$–0.027 according to NED). Kowalski et al. (1992) reported a 2σ upper limit for the X-ray luminosity $L_X(2\text{–}6\,\mathrm{keV}) = 0.58\times10^{44}\,h_{75}^{-2}\,\mathrm{erg\,s^{-1}}$ (in their cosmology).

We identified the well known bright radio source B2 0756+27 (ID 91 in our catalog, see below) as a double radio galaxy associated with the optically brightest, giant elliptical of the cluster (Valentijn 1979; see also Owen et al. 1992). For this galaxy Owen et al. (1995) measured a redshift of $z = 0.0991 \pm 0.0002$ and detected Hα+NII emission lines. This WAT radio galaxy has been recently studied by Jetha et al. (2006), too. The presence of a diffuse radio source at Southeast from the radio galaxy (see Fig. 1) was suggested by Valentijn (1979) and then confirmed and classified as a relic by Giovannini & Feretti (2000).

Table 1 lists our velocity catalog and Fig. 2 shows the finding chart for the 165 galaxies in the field of A610. In Table 1, for each galaxy we provide: identification number ID (Col. 1), right ascension and declination, α and δ (J2000, Col. 2); r' SDSS magnitudes (Col. 3); heliocentric radial velocities, $v = cz_\odot$ (Col. 4) with errors, Δv (Col. 5); source of velocity data (W: WHT, S: SDSS, W+S: combined WHT and SDSS) in Col. 6.

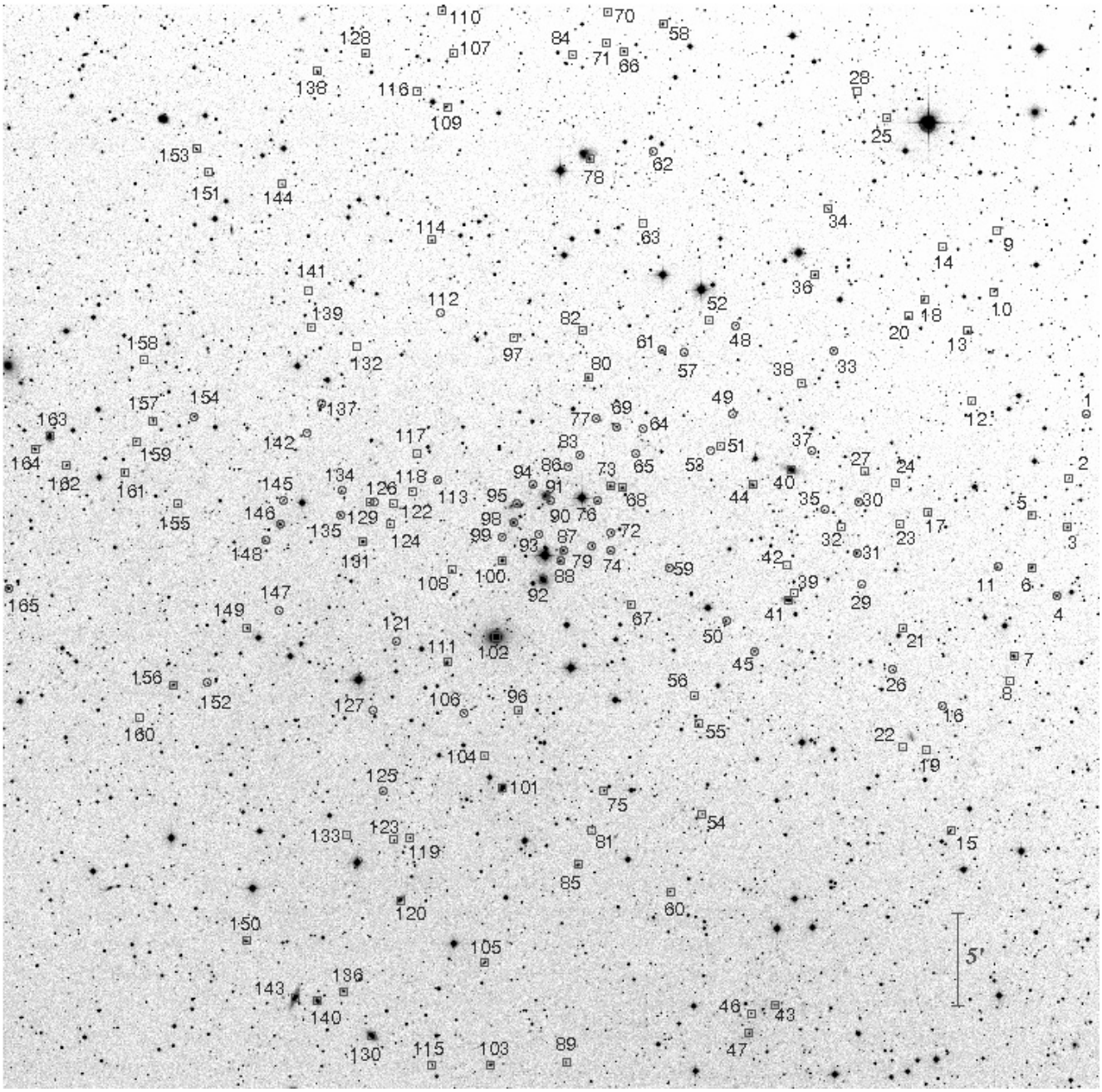

Fig. 2. DSS2 *R*-band image of A610 (*North at the top and East to the left*). Galaxies with successful velocity measurements are labeled as in Table 1. Circles and boxes indicate cluster members and non-member galaxies, respectively.

The typical error on radial velocity as given by the median value is 38 km s^{-1}.

3.1. Member selection and global properties

To select cluster members from the 165 galaxies having redshifts, we use the adaptive-kernel method (hereafter DEDICA, Pisani 1993, 1996; see also Fadda et al. 1996; Girardi et al. 1996; Girardi & Mezzetti 2001). We find significant peaks in the velocity distribution at >99% c.l. This procedure detects A610 as a one-peaked structure, populated by 61 galaxies with $27\,598 \leq v \leq 31\,213$ km s^{-1} (see Fig. 3). Out of the non-member galaxies, 70 and 34 are foreground and background galaxies, respectively.

All the galaxies assigned to the A610 peak are analyzed in the second step, which uses the combination of position and velocity information. We apply the procedure of the "shifting gapper" by Fadda et al. (1996). This procedure rejects galaxies that are too far in velocity from the main body of galaxies and within a fixed bin that shifts along the distance from the cluster center. The procedure is iterated until the number of cluster members converges to a stable value. Following Fadda et al. (1996) we use a gap of 1000 km s^{-1} in the cluster rest-frame and a bin of 0.6 h_{70}^{-1} Mpc, or large enough to include 15 galaxies. As for the cluster center, we consider the position of the dominant galaxy (RA = $07^{h}59^{m}17^{s}.10$, Dec = $+27°09'16''.1$ (J2000)) which was identified with the radio galaxy producing the source B2 0756+27 (see above). The shifting-gapper procedure rejects another four galaxies as non-members (cross

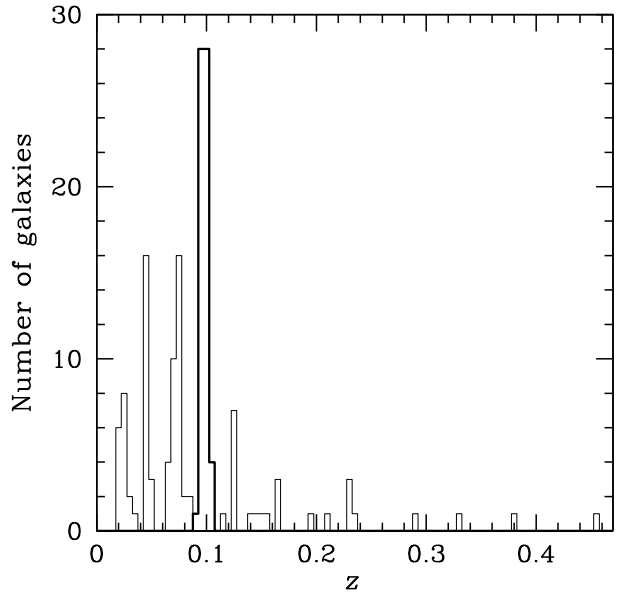

Fig. 3. A610: redshift galaxy distribution. The solid line histogram refers to galaxies assigned to the cluster according to the DEDICA reconstruction method.

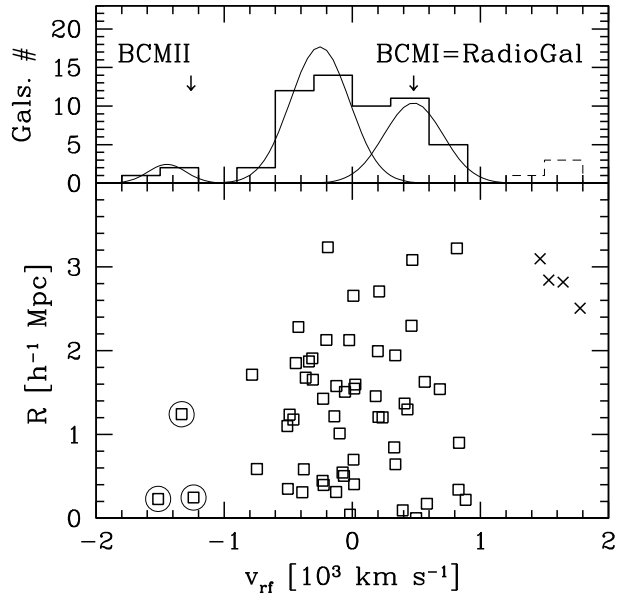

Fig. 4. A610. *Bottom panel*: rest-frame velocity vs. projected cluster-centric distance for the 61 galaxies in the main peak (Fig. 3) showing galaxies detected as interlopers by our "shifting gapper" procedure (crosses). Squares indicate galaxies forming the sample of the 57 member galaxies. The three galaxies with the lowest velocities are rejected to build Sample2 (see text). *Top panel*: velocity distribution of the 57 cluster members and 4 rejected galaxies (solid and dashed histograms). Arrows correspond to the two brightest cluster members. The three Gaussians correspond to the three KMM groups (see Table 2).

symbols in Fig. 4). Thus, the member selection procedure leads to a sample of 57 cluster members (see Table 1 and Fig. 4).

By applying the biweight estimator to the cluster members (Beers et al. 1990), we compute a mean cluster redshift of $\langle z \rangle = 0.0976 \pm 0.0002$, i.e., $\langle v \rangle = 29\,255 \pm 66$ km s^{-1}. We estimate the LOS velocity dispersion, σ_V, by using the biweight estimator and applying the cosmological correction and the standard correction for velocity errors (Danese et al. 1980). We

Table 2. A610: results of the kinematical analysis.

Sample	N_g	$\langle v \rangle$ km s^{-1}	σ_V^a km s^{-1}	R_{vir} Mpc	Mass($<R_{vir}$) 10^{14} $M_\odot$
Whole system	57	$29\,255 \pm 66$	496^{+73}_{-48}	1.15	$2.3^{+0.8}_{-0.5}$
Whole system Sample2	54	$29\,283 \pm 58$	426^{+38}_{-39}	0.99	$1.8^{+0.4}_{-0.4}$
Virialized subsample	22	$29\,312 \pm 106$	480^{+71}_{-59}	1.11	$1.8^{+0.6}_{-0.5}$
KMM1	3	$27\,766 \pm 89$	(118)	–	–
KMM2	34	$29\,017 \pm 40$	227^{+38}_{-21}	0.53	$0.22^{+0.09}_{-0.07}$
KMM3	20	$29\,767 \pm 54$	235^{+32}_{-29}	0.54	$0.25^{+0.09}_{-0.07}$

[a] We use the biweigth estimator by Beers et al. (1990). For the sample with 3 galaxies we indicate the standard dispersion estimate.

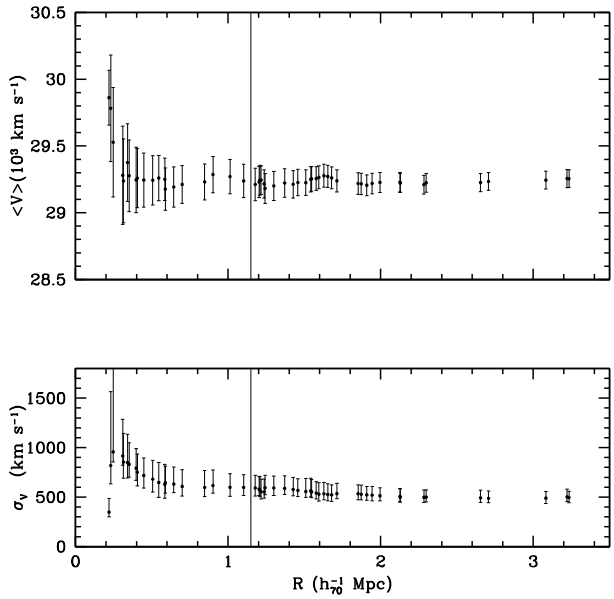

Fig. 5. A610: integral profiles of mean velocity and LOS velocity-dispersion are shown in *top and bottom panels*, respectively. The mean and dispersion at a given (projected) radius from the cluster center is estimated by considering all galaxies within that radius – the first value computed on the five galaxies closest to the center. The error bands at the 68% c.l. are also shown. The faint vertical lines give the radius of the virialized region.

obtain $\sigma_V = 496^{+73}_{-48}$ km s^{-1}, where errors are estimated through a bootstrap technique.

Here we compute the mass of A610 assuming that the system is in dynamical equilibrium. Following the prescriptions of Girardi & Mezzetti (2001) – in particular see their Eq. (1) after introducing the scaling with $H(z)$ – we assume for the radius of the quasi-virialized region $R_{vir} = 0.17 \times \sigma_V / H(z) = 1.15\ h_{70}^{-1}$ Mpc (see also Eq. (8) of Carlberg et al. 1997 for R_{200}). Therefore, our spectroscopic catalog samples the whole virialized region of the cluster.

One can compute the mass using the virial theorem (Limber & Mathews 1960; see also Girardi et al. 1998) under the assumption that mass follows galaxy distribution: $M = 3\pi/2 \cdot \sigma_V^2 R_{PV}/G$ is the standard virial mass, R_{PV} a projected radius (equal to two times the harmonic radius). Figure 5 shows that the estimate of σ_V is robust when computed within a large cluster region, thus we consider the global value (see Fig. 5 of Girardi et al. 2006; and Fadda et al. 1996, for other examples). The value of R_{PV} depends on the size of the region considered so that the computed mass increases (but not linearly) with the increasing region

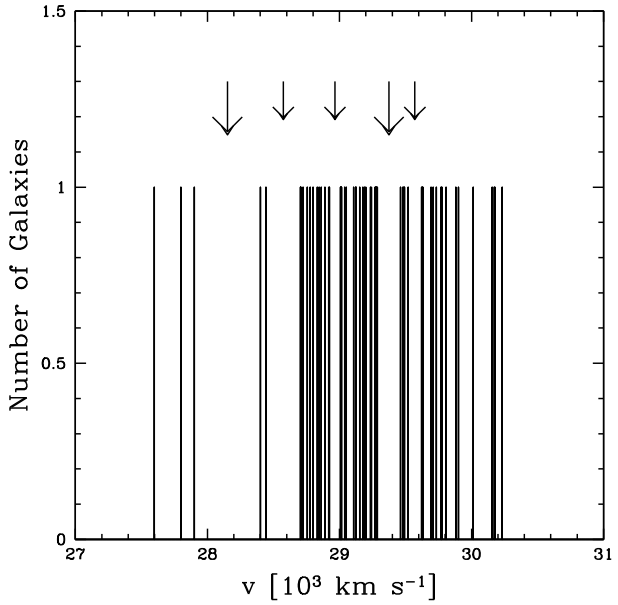

Fig. 6. A610: stripe density plot where the arrows indicate the positions of the significant gaps. The two most important gaps are indicated by the two big arrows.

considered. Considering the 24 galaxies within $R_{\rm vir}$ we obtain $R_{\rm PV} = 0.87 \pm 0.11\ h_{70}^{-1}$ Mpc .

We obtain a virial mass $M(<R_{\rm vir} = 1.15\ h_{70}^{-1}\,{\rm Mpc}) = 2.3^{+0.8}_{-0.6} \times 10^{14}\ h_{70}^{-1}\ M_{\odot}$. Notice that in this case we do not apply the 20% surface pressure term correction (e.g., The & White 1986; Carlberg et al. 1997; Girardi et al. 1998) since we use the value of the velocity dispersion as computed within a very large radius.

We also consider an alternative sample of 54 galaxies – Sample2 – rejecting the three galaxies with lowest velocity, which are separated by a gap of ~450 km s^{-1} in the reference frame from the whole velocity distribution of the cluster (see Fig. 4). Since this is a poor cluster such a value for a gap is quite anomalous (see also below Sect. 3.2). The properties of Sample2 are listed in Table 2.

We also present the analysis of the 22 galaxies which are the subsample of Sample2 contained within $R_{\rm vir}$ (hereafter the "virialized subsample"), to consider galaxies likely belonging to the true internal, virialized structure.

3.2. Analysis of the spectroscopic sample

We analyze the velocity distribution to look for possible deviations from Gaussianity that could provide important signatures of complex dynamics. For the following tests the null hypothesis is that the velocity distribution is a single Gaussian.

We estimate three shape estimators, i.e., the kurtosis, the skewness, and the scaled tail index (see, e.g., Beers et al. 1991). The value of the skewness (−0.530) shows a marginal evidence that the velocity distribution differs from a Gaussian at the 90–95% c.l. (see Table 2 of Bird & Beers 1993). Moreover, the W-test (Shapiro & Wilk 1965) marginally rejects the null hypothesis of a Gaussian parent distribution at the 90% c.l. The analysis of Sample2 also shows a marginal sign of non-Gaussianity having the kurtosis a value of 3.693 (at 90–95% c.l.).

Then we investigate the presence of gaps in the velocity distribution. A weighted gap in the space of the ordered velocities

Table 3. A610: results of the weighted-gap analysis.

Sample	$N_{\rm gals,prec}$	$v_{\rm prec}$ km s^{-1}	Size	Prob.of.detect.
Whole sample	3	27 901	2.79	6.0E-3
Whole sample	5	28 444	2.55	1.4E-2
Whole sample	17	28 924[a]	2.32	3.0E-2
Whole sample	36	29 287[a]	3.56	5.0E-4
Whole sample	5	29 521[a]	2.73	1.4E-2
Virialized sample	14	29 277[b]	3.19	2.0E-3

[a] Gaps also found in Sample2.
[b] This gap corresponds to the most significant in the whole sample.

is defined as the difference between two contiguous velocities, weighted by the location of these velocities with respect to the middle of the data. We obtain values for these gaps relative to their average size, precisely the midmean of the weighted-gap distribution. We look for normalized gaps larger than 2.25 since in random draws of a Gaussian distribution they arise at most in about 3% of the cases, independently of the sample size (Wainer and Schacht 1978; see also Beers et al. 1991). We find five significant gaps (see Fig. 6), the main one lying in the body of the distribution at $v \sim 29\,500$ km s^{-1} and the secondary one separates the three galaxies with the lowest velocity from the body of the velocity distribution. In Table 3 we list the number of galaxies and the velocity of the object preceding the gap, the normalized size (i.e., the "importance") of the gap itself, and the probability of finding a normalized gap of this size with the same position in a normal distribution (as computed with ROSTAT package, Beers et al. 1990). The importance of the main gap is confirmed by the analysis of Sample2.

We use the results of the gap analysis to determine the first guess when using the Kaye's mixture model (KMM) to find a possible group partition of the velocity distribution (as implemented by Ashman et al. 1994). The KMM algorithm fits an user-specified number of Gaussian distributions to a dataset and assesses the improvement of that fit over a single Gaussian. In addition, it provides the maximum-likelihood estimate of the unknown n-mode Gaussians and an assignment of objects into groups. KMM is most appropriate in situations where theoretical and/or empirical arguments indicate that a Gaussian model is reasonable. The Gaussian is valid in the case of cluster velocity distributions, where gravitational interactions drive the system toward a relaxed configuration with a Gaussian velocity distribution. However, one of the major uncertainties of this method is the optimal choice of the number of groups for the partition. Using the results of the gap analysis we try to fit two and three velocity groups on the basis of the two most important gaps.

We find that a two-groups partition is a significantly better descriptor of the velocity distribution with respect to a single Gaussian at the 90–92% c.l. (homoscedastic and heteroscedastic cases) where the first group is given by the three lowest velocity galaxies. Moreover, we find a significant three-groups partition of 3–34–20 galaxies (at the 96.8% c.l. in the homoscedastic case). The KMM analysis of Sample2 confirms the presence of the two groups with 34 and 20 galaxies (at the ~90% c.l.). Table 2 lists the results for the kinematical analysis of the groups with 3, 34, and 20 galaxies and Fig. 4 shows the corresponding Gaussians. We also list the virial radii and masses of the groups KMM2 and KMM3. They are computed assuming the dynamical equilibrium and adopting an alternative estimate for $R_{\rm PV}$ useful when the centers of the systems are not well defined (see Barrena et al. 2007b, their Sect. 4). However, we point out that

the uncertainty in KMM membership assignments leads to an artificial truncation of the tails of the velocity distributions, thus the velocity dispersions of the two groups are underestimated (see Bird 1994). As a consequence, the masses of KMM2 and KMM3 should be considered only approximated lower limits.

Notice that the first and the second brightest galaxies of the cluster (galaxy IDs 91 and 99; hereafter we refer to them as BCMI and BCMII) are assigned to KMM3 and KMM1 groups. In particular, BCMI has a velocity very close to the mean velocity of its host KMM3 system, while it shows evidence of peculiarity according to the Indicator test by Gebhardt & Beers (1991, at the >95% c.l.) with respect to the whole system. As for KMM2, it does not host very luminous galaxies. Indeed, not all galaxy systems are characterized by particularly bright galaxies. In particular, dominant galaxies are often absent in poorly evolved structures (see, for instance, the "irregular" and "flat" clusters according to the definition of Struble & Rood 1982, 1984). The existence of a correlation between positions and velocities of cluster galaxies is a footprint of real substructures. To investigate the velocity field of the A610 complex we divide galaxies in a low and a high velocity samples by using the median cluster velocity and check the difference between the two distributions of galaxy positions. The two distributions are different at the 92.3% c.l. according to the 2DKS-test. The same analysis on Sample2 leads to a difference at the 98.4% c.l. In order to estimate the direction of the velocity gradient we perform a multiple linear regression fit to the observed velocities with respect to the galaxy positions in the plane of the sky (see also den Hartog & Katgert 1996; Girardi et al. 1996). We find a position angle on the celestial sphere of PA = 184^{+25}_{-19} degree (measured counter-clockwise from north, i.e., higher-velocity galaxies lie in the southern region), but marginally significant (at the 90% c.l.).

Looking for a correlation between positions and velocities, we also compare the KMM groups two-by-two by applying the 2DKS-test to the galaxy position of member galaxies. When comparing KMM2 with KMM3 we obtain a difference at the 99.88% c.l. and a marginal difference when comparing KMM1 with KMM2 (at the 90% c.l.). Figure 7 shows as the higher velocity KMM3 group lies SW with respect KMM2 group.

When limiting our analysis to the "virialized subsample" we find again: a marginal evidence of non-Gaussianity (at the 90–95% c.l. from the kurtosis of −0.849); the gap at ∼29 500 km s^{-1}; a different spatial distribution between low and high velocity populations (at the ≳95% c.l.). The presence of a velocity gradient is now significant at the 94% c.l. with a value of PA = 64^{+59}_{-42} and, in fact, the high velocity KMM3 galaxies lie NE in the central cluster region (see Fig. 7).

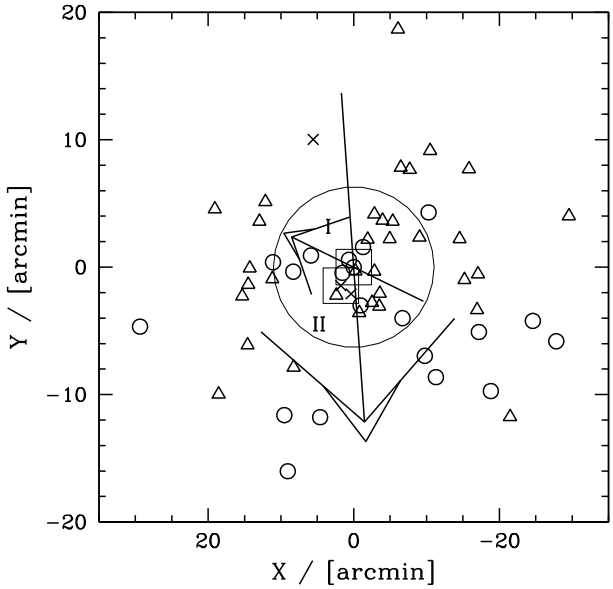

Fig. 7. A610: spatial distribution on the sky of the 57 cluster members. KMM1, KMM2 and KMM3 galaxies are denoted by crosses, triangles and circles, respectively. The position of the two brightest galaxies (BCMI and BCMII) are indicated by the faint large squares. The circle indicates the likely virialized region. Bigger and smaller arrows indicate the velocity gradients within the whole and the virialized regions, respectively. The plot is centered on the cluster center defined as the position of BCMI.

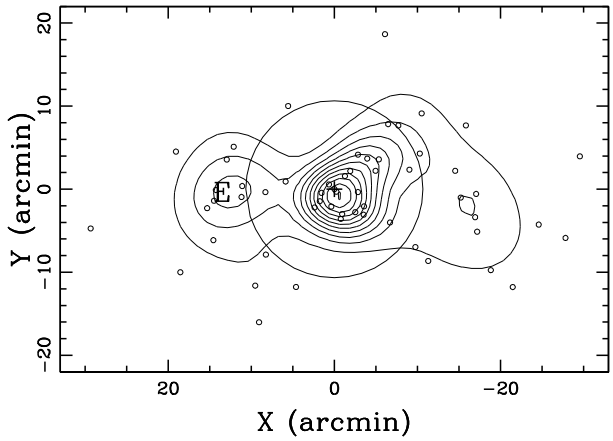

Fig. 8. A610: spatial distribution on the sky of spectroscopically confirmed cluster members and the relative isodensity contour map. The brightest cluster member BCMI is indicated by a cross. The circle indicates the likely virialized region. The Eastern peak is indicated, too. The plot is centered on the cluster center defined as the position of BCMI.

3.3. 2D galaxy distribution

When applying the DEDICA method to the 2D distribution of the 57 cluster members we find two very significant peaks (at the >99.9 c.l., see Fig. 8). The position of the highest peak is close to the location of the brightest cluster member. The secondary peak lies at ∼15′ East (∼1.6 h_{70}^{-1} Mpc) with respect to the BCMI. We compare the mean velocity of galaxies belonging to the main peak of our 2D analysis with that of galaxies belonging to the eastern secondary peak. We find no difference. This explains why the eastern structure is not detected in the analyses of Sect. 3.2.

Our spectroscopic data suffer from magnitude incompleteness. To overcome this limit we recover the photometric catalog extracted from the SDSS DR5.

The color–magnitude relation (hereafter CMR), which indicates the early-type galaxy locus, is usually applied to select likely cluster members (see, e.g., A725 in this paper and references therein). When more than two colors are available, it is more effective to select galaxies in color-color space. Here we consider the $i'-z'$ vs. $r'-i'$ plane where a rectangular box seems suitable for galaxy selection (e.g., Fig. 12 by Goto et al. 2002). In particular, we consider likely members galaxies having r' within 0.08 mag from $r'-i' = 0.41$ and $i'-z' = 0.32$, i.e., the median values recovered from the spectroscopically cluster members (see Fig. 9). The value of 0.08 mag is about two times the typical scatter reported by Goto et al. (2002) for the two CMRs $r'-i'$ vs. r' and $i'-z'$ vs. r'. To avoid contamination

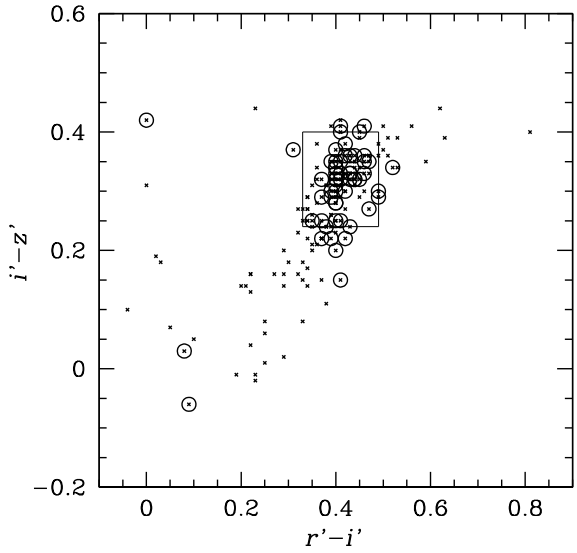

Fig. 9. A610: i'–z' vs. r'–i' diagram for galaxies with available spectroscopy is shown by small crosses. The faint square is centered on the median value for colors of member galaxies (circles) and encloses galaxies having colors in the range of 0.08 mag from median values.

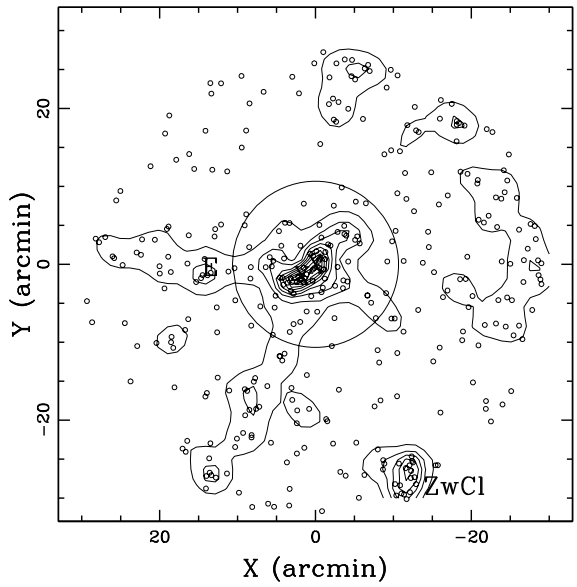

Fig. 10. A610: spatial distribution on the sky and relative isodensity contour map of the 357 likely cluster members (according to the color–color diagram) with $r' \leq 20$, obtained with the DEDICA method. BCMI and BCMII are indicated by crosses. The circle indicates the likely virialized region. The Eastern peak and the Zw Cl0755.2+2649 are indicated, too.

by field galaxies we do not show results for galaxies fainter than 20 mag (in r'-band).

The contour map for the 357 likely cluster members having $r' \leq 20$ is shown in Fig. 10. We also analyze galaxies likely members having $r' \leq 19$ and $19 < r' \leq 20$ in a separate way. Our general results are the following. We confirm the presence of the eastern peak, which is generated by bright galaxies. The main structure, contained in the virialized region, shows a much more complex structure having two peaks centered around BCMII and BCMI.

Finally, we notice that the southern peak detected at the southern border of the field is Zwicky Cluster 0755.2+2649

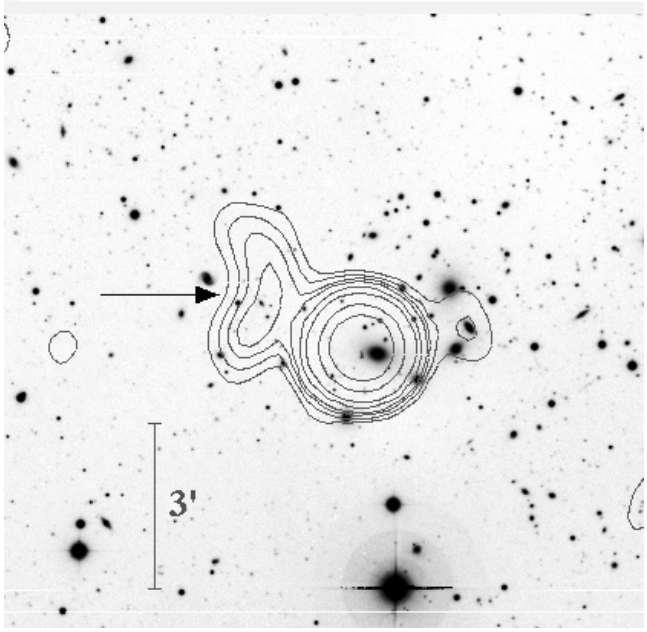

Fig. 11. *R*-band image of A725 (data taken with the WFC camera of the INT) with, superimposed, the contour levels of a radio image from the Westerbork Northern Sky Survey (WENSS, see Kempner & Sarazin 2001). The arrow shows the position of the radio relic. *North is at the top and East to the left.*

(recognized by NED as the RXCJ 0758.3 at $z = 0.2315$, Böhringer et al. 2000).

4. Abell 725

A725 is a poor Abell cluster (Abell richness class = 0). It is characterized by an irregular/clumpy galaxy distribution and a low X-ray luminosity $L_X(0.1\text{–}2.4\ \mathrm{keV}) = 0.80 \times 10^{44}\, h_{50}^{-2}\ \mathrm{erg\,s^{-1}}$ (Böhringer et al. 2000 in their cosmology).

The brightest radio source in the cluster (see Fig. 11) is associated with the bright elliptical in the cluster center at $z = 0.0900 \pm 0.0002$ (Owen et al. 1993, 1995). The relic is seen as an arc of diffuse emission to the northeast of this source (Kempner & Sarazin 2001). Kempner & Sarazin also noticed that the X-ray gas as seen in the ROSAT All-Sky Survey is slightly elongated along the axis connecting the relic and the cluster center.

Table 4 lists our velocity catalog and Fig. 12 shows the finding chart for the 51 galaxies in the field of A725. In Table 4, for each galaxy, we provide: identification number ID (Col. 1), right ascension and declination, α and δ (J2000, Col. 2); R and B Johnson magnitudes (Cols. 3 and 4); heliocentric radial velocities, $v = cz_\odot$ (Col. 5) with errors, Δv (Col. 6). The typical error on the radial velocity as given by the median value is 68 km s^{-1}.

4.1. Member selection and analysis

Out of 51 galaxies in the sample, the DEDICA method detects A725 as a one-peaked structure, populated by 36 galaxies with $25\,973 \leq v \leq 29\,360$ km s^{-1} (see Fig. 13). Out of the 15 non-member galaxies, 5 and 10 are foreground and background galaxies, respectively.

As for the cluster center, we consider the position of the brightest cluster member (BCMI; ID 24 in the velocity catalog), which was identified with the radio galaxy producing the brightest radio source (see above). No galaxy is rejected by the

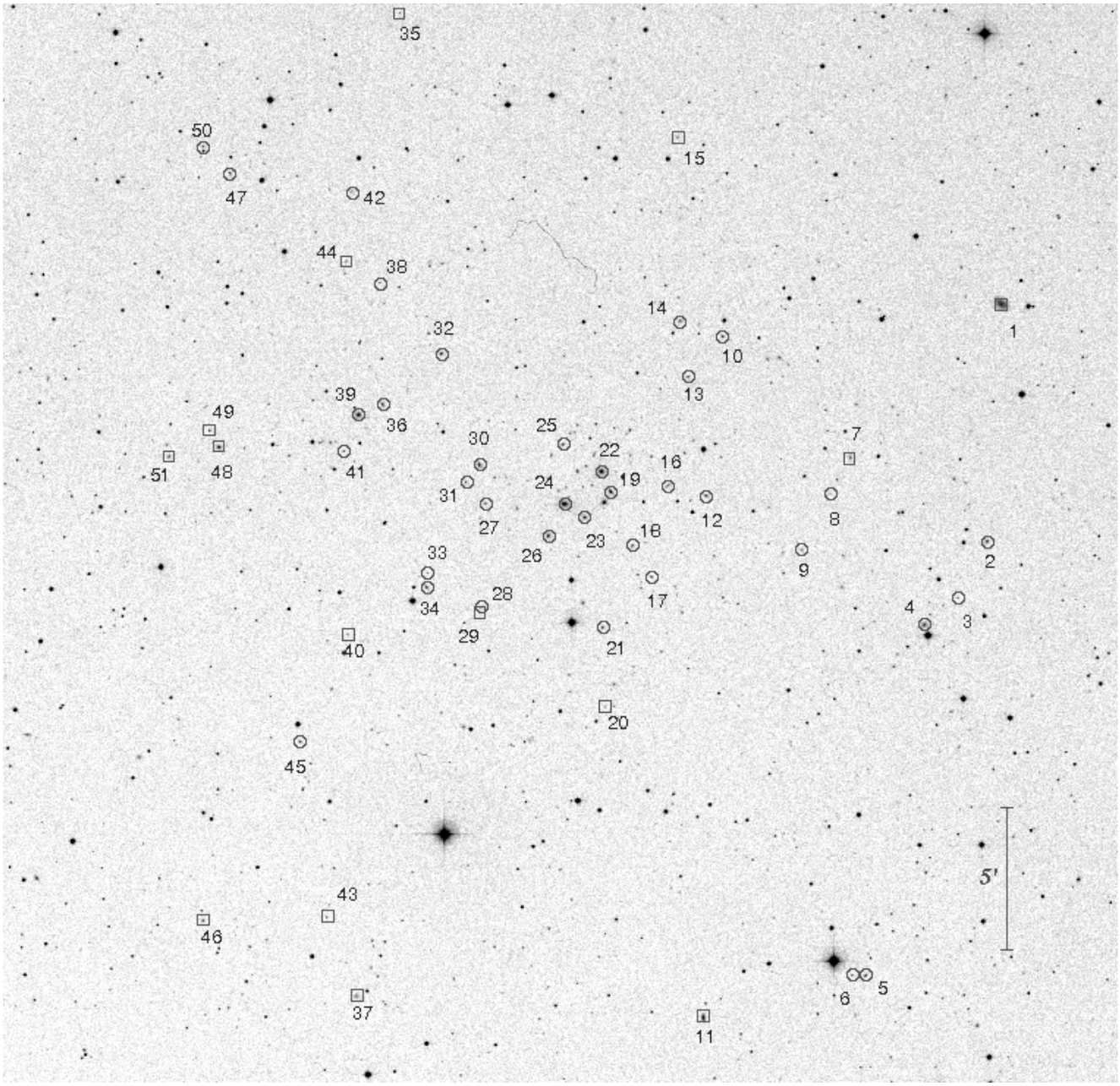

Fig. 12. DSS2 *R*-band image of A725 (*North at the top and East to the left*). Galaxies with successful velocity measurements are labeled as in Table 4. Circles and boxes indicate cluster members and non-member galaxies, respectively.

"shifting gapper" leading to a sample of 36 cluster members (see Table 4 and Fig. 14).

By applying the biweight estimators to cluster members (Beers et al. 1990), we compute a mean cluster redshift of $\langle z \rangle = 0.0917 \pm 0.0003$, i.e., $\langle v \rangle = 27\,478 \pm 90$ km s^{-1} and $\sigma_V = 534^{+132}_{-97}$ km s^{-1}. Assuming that the system is in dynamical equilibrium we compute for the radius of the virialized region $R_{\rm vir} = 1.24\ h_{70}^{-1}$ Mpc and $M(<R_{\rm vir} = 1.24\ h_{70}^{-1}$ Mpc) $= 3.2^{+1.6}_{-1.2} \times 10^{14}\ h_{70}^{-1}\ M_\odot$.

The values of the kurtosis (3.998) and the scaled tail index (1.504) indicate that the velocity distribution is lighter-tailed than a Gaussian at the 90–95% and the 95–99% c.l.s (see Table 2 of Bird & Beers 1993), respectively. The BCMI shows evidence of peculiarity, according to the Indicator test by Gebhardt & Beers (1991, at the >95% c.l.), with respect to the whole system. We do not find any other trace of substructure.

In this cluster, we find evidence of luminosity segregation. For the 33 galaxies having available magnitude, the magnitude *R* correlates with the clustercentric distance at the 99.5% c.l., according to the Spearman correlation coefficient.

4.2. 2D galaxy distribution

By applying the DEDICA method to the 2D distribution of A725 cluster members we find that the cluster is elongated along the EW direction.

We recover our photometric catalog selecting likely members on the basis of the $B-R$ vs. R relation (see, e.g., Barrena et al. 2007b). To determine the relation we fix the slope according to López-Cruz et al. (2004, see their Fig. 3) and apply the two-sigma-clipping fitting procedure to the cluster members obtaining $B-R = 2.971-0.054 \times R$. In our photometric catalog we

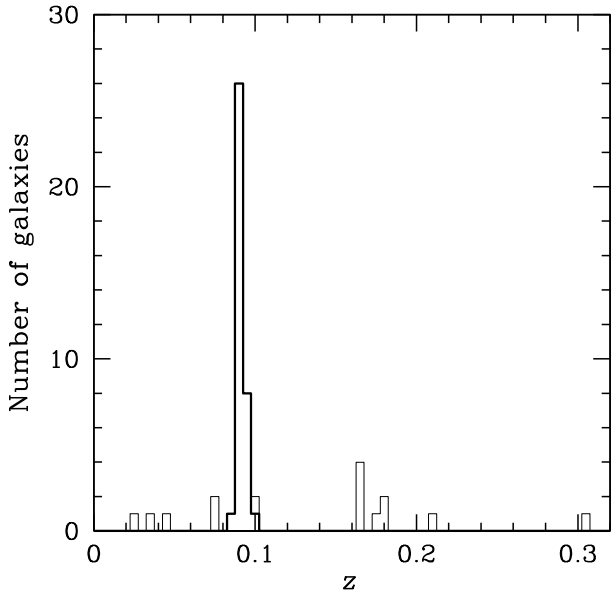

Fig. 13. A725: redshift galaxy distribution. The solid line histogram refers to galaxies assigned to the cluster according to the DEDICA reconstruction method.

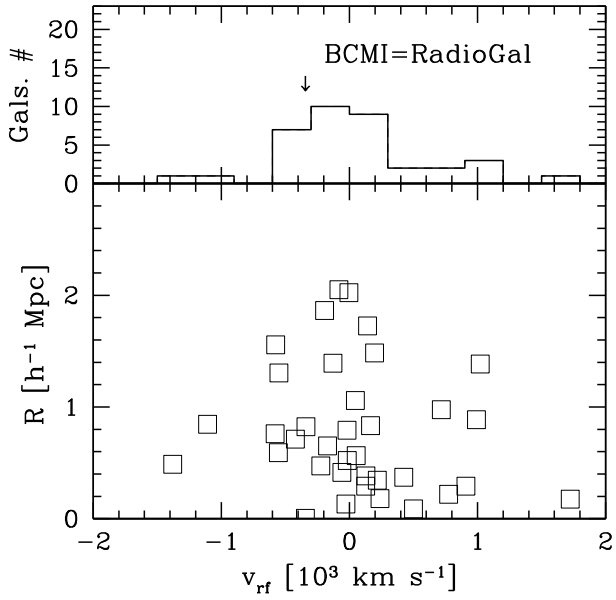

Fig. 14. A725: *Bottom panel*: rest-frame velocity vs. projected cluster-centric distance for the 36 member galaxies. *Top panel*: velocity distribution of 36 cluster members. The arrow corresponds to the brightest cluster member.

consider galaxies (objects with SExtractor stellar index ≤0.9) lying within 0.25 mag of the relation. To avoid contamination by field galaxies we do not show results for galaxies fainter than 20 (in the *R*-band).

The contour map for the 360 likely cluster members having $R \leq 20$ is elongated along the E-W direction in the central region and the position of the density peak lies about 2′ from the BCMI, assumed as cluster center (see Fig. 15). Moreover, the cluster shows an important secondary peak towards NE and the cluster itself appear elongated along the NE-SW direction (see the isodensity contours at the virial radius distance). Similar features are obtained analyzing other magnitudes cuts ($R \leq 19$ or $R \leq 18$).

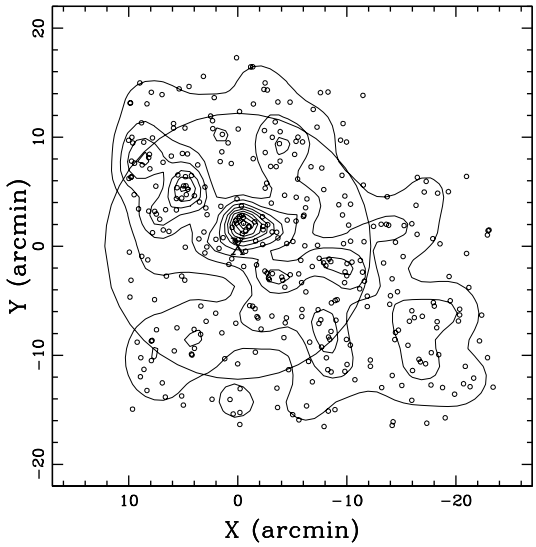

Fig. 15. A725: spatial distribution on the sky and relative isodensity contour map of the 360 likely cluster members (according to the two colors selection) with $R \leq 20$, obtained with the DEDICA method. The cross indicates the BCMI. The circle indicates the likely virialized region.

5. Abell 796

A796 is an Abell cluster of Abell richness class = 1. It is characterized by a clumpy galaxy distribution and a low X-ray luminosity $L_X(0.1\text{–}2.4\ \mathrm{keV}) = 1.38 \times 10^{44}\ h_{50}^{-2}\ \mathrm{erg\,s^{-1}}$ (Kempner & Sarazin 2001 in their cosmology).

Kempner & Sarazin (2001) found a centrally-located diffuse radio emission which is quite large and has a very low surface brightness. When converting in our cosmology the X-ray luminosity and the radio halo power by Kempner & Sarazin (2001), we find $L_X(0.1\text{–}2.4\ \mathrm{keV}) = 0.93 \times 10^{44}\ h_{70}^{-2}\ \mathrm{erg\,s^{-1}}$ and $P_{1.4\,\mathrm{GHz}} = (5.6 \pm 2.1) \times 10^{23}\ \mathrm{W\,Hz^{-1}}$, respectively. These nominal values stay far from the correlation between radio power and X-ray luminosity as given by Cassano et al. (2006, see their Fig. 1). However, the halo is uncertain and the error on the radio power is so large that deeper imaging is needed to confirm the presence of the radio halo and to measure its flux with greater precision. Owen et al. (1993) found two close radio galaxies in the field of this cluster. The radio source A is here identified with a background AGN (ID 65 at $z \sim 0.295$ in our catalog, see below), while we have no z for the radio source B.

Table 5 lists our velocity catalog, and Fig. 16 shows the finding chart for the 99 galaxies in the field of A796. In Table 5, for each galaxy we provide: identification number ID (Col. 1), right ascension and declination, α and δ (J2000, Col. 2); r' SDSS magnitudes (Col. 3); heliocentric radial velocities, $v = cz_\odot$ (Col. 4) with errors, Δv (Col. 5); source of velocity data (W: WHT, S: SDSS, W+S: combined WHT and SDSS) in Col. 6. The typical error on radial velocity as given by the median value is 45 km s^{-1}.

5.1. Member selection and analysis

Out of 99 galaxies in the sample, the DEDICA method detects A796 as a one-peaked structure, populated by 27 galaxies with $45\,242 \leq v \leq 50\,023$ km s^{-1} (see Fig. 17). Out of the non-member galaxies, 38 and 34 are foreground and background galaxies, respectively.

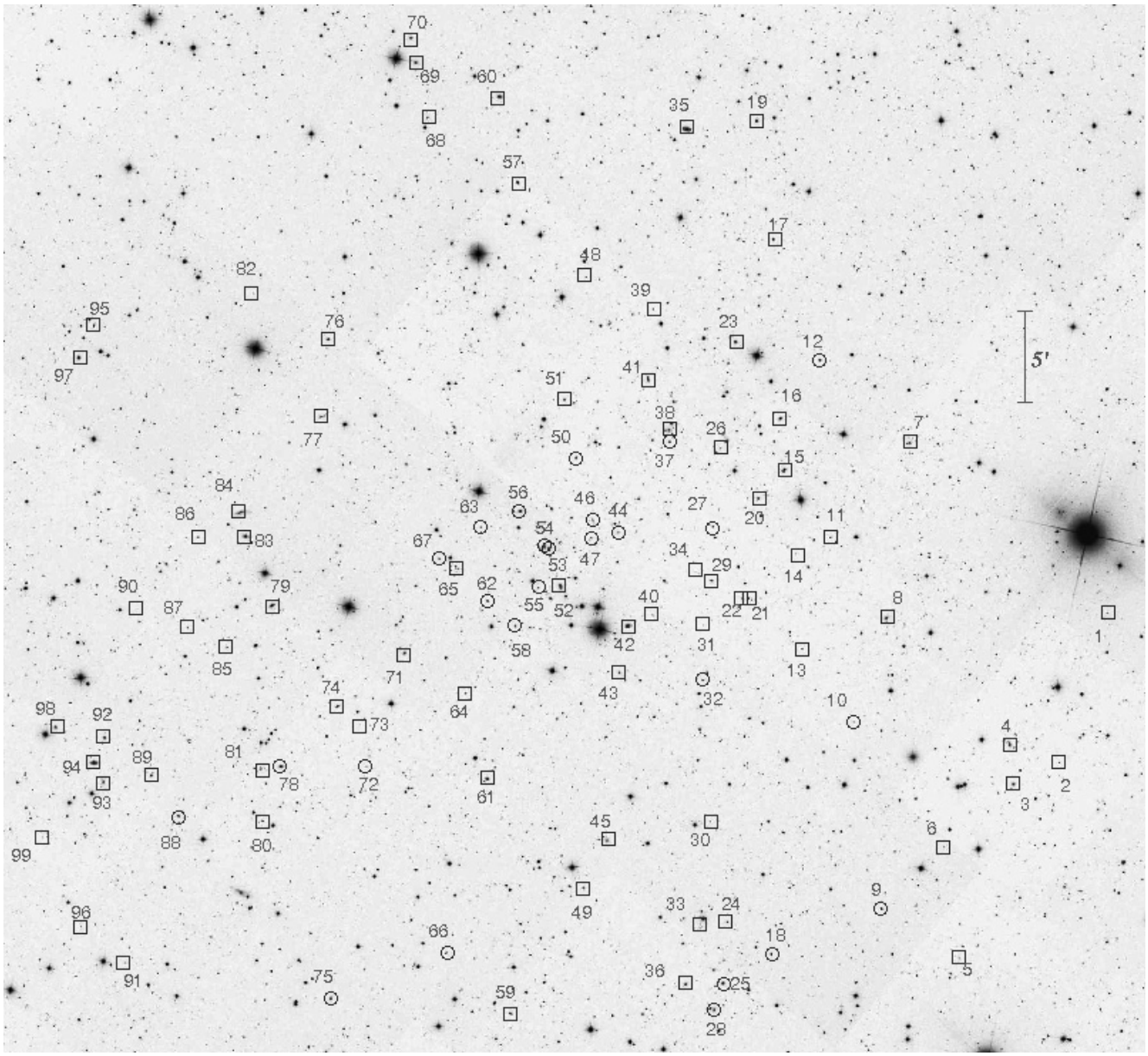

Fig. 16. SDSS image of A796 (*North at the top and East to the left*). Galaxies with successful velocity measurements are labeled as in Table 5. Circles and boxes indicate cluster members and non-member galaxies, respectively.

As for the cluster center, we consider the position of the peak in the 2D galaxy distribution as determined by the 2D DEDICA method (RA = $09^h27^m57^s.55$, Dec = +60°26′33″.7 (J2000)]. Only one galaxy is then rejected by the "shifting gapper" leading to a sample of 26 cluster members (see Table 5 and Fig. 18).

Figure 18 also shows the velocity (with respect to the cluster mean) of the two luminous cluster galaxies, IDs 56 and 54. They have a comparable r' magnitude, but while ID 54 lies somewhat closer to the cluster center, ID 56 lies $\lesssim 0.4\ h_{70}^{-1}$ Mpc from the cluster center. Hereafter, we refer to IDs 56 and 54 as BCMInc and BCMI, respectively.

By applying the biweight estimators to 26 cluster members (Beers et al. 1990), we compute a mean cluster redshift of $\langle z \rangle = 0.1566 \pm 0.0005$, i.e., $\langle v \rangle = 46\,942 \pm 140$ km s^{-1} and $\sigma_V = 698^{+216}_{-159}$ km s^{-1}. Assuming that the system is in dynamical equilibrium we compute for the radius of the virialized region $R_{vir} = 1.57\ h_{70}^{-1}$ Mpc and the virial mass $M(<R_{vir} = 1.57\ h_{70}^{-1}\ \text{Mpc}) = 6.9^{+4.0}_{-3.0} \times 10^{14}\ h_{70}^{-1}\ M_\odot$.

We also consider an alternative sample of 24 galaxies – Sample2 – rejecting the two galaxies with the highest velocity that are separated by a gap of ~820 km s^{-1} in the reference frame from the whole velocity distribution of the cluster (see Fig. 18). This gap is detected with a significance level of (1–3.0E–2) in the velocity distribution (see Fig. 19). The properties of Sample2 are listed in Table 6.

We also present the analysis of the 14 galaxies which are the subsample of Sample2 contained within R_{vir} (hereafter the "virialized subsample") to consider galaxies likely belonging to the true internal, virialized structure.

Considering the whole sample of 26 galaxies we find the presence of a velocity gradient at the 98.9% c.l., with high velocity galaxies SSE located (PA = 156^{+21}_{-26}). Accordingly, the two subsamples of galaxies having lower or higher velocity than the median velocity show different distributions in the sky (at the 99.5% according to the 2DKS test). Moreover, the Dressler-Schectman test finds substructure at the 96% c.l. However, these

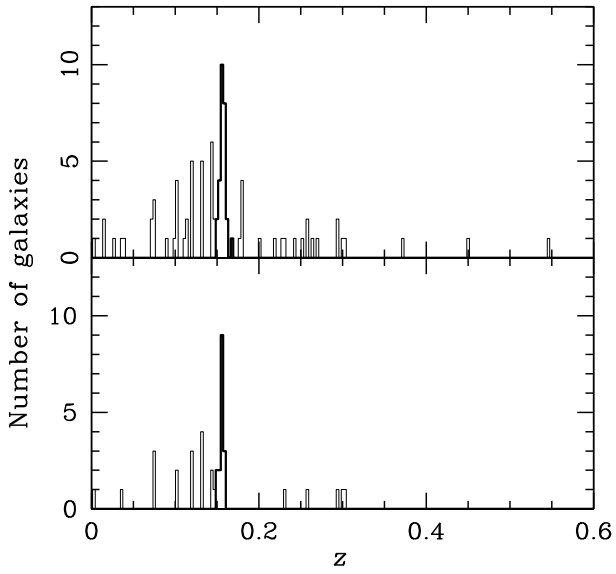

Fig. 17. A796: redshift galaxy distribution of only galaxies with $z < 0.6$. *Top panel.* Whole catalog: the solid line histogram refers to galaxies assigned to the cluster according to the DEDICA reconstruction method. *Bottom panel.* The same for galaxies within 15′ from the cluster center.

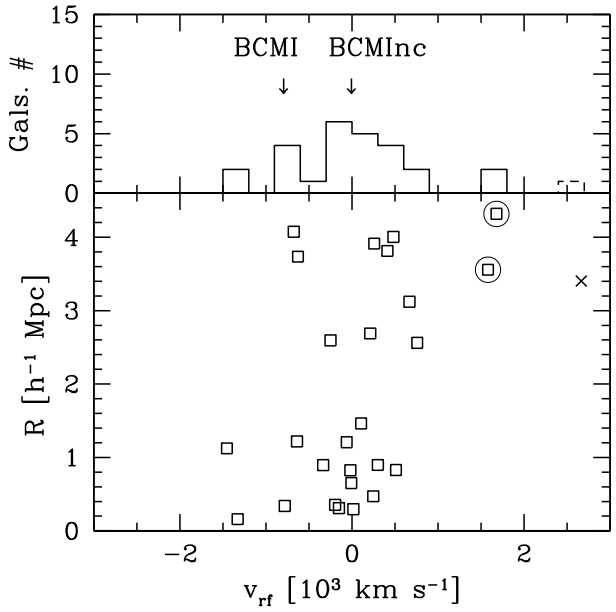

Fig. 18. A796: *Bottom panel*: rest-frame velocity vs. projected cluster-centric distance for the 27 galaxies in the main peak (Fig. 3) showing galaxies detected as interloper by our "shifting gapper" procedure (crosses). Squares indicate galaxies forming the sample of member galaxies. The two galaxies with the highest velocities are rejected to build Sample2 (see text). *Top panel*: velocity distribution of the 26 cluster members and the rejected galaxy (solid and dashed histograms). Arrows correspond to the two luminous member galaxies.

pieces of evidence of correlation between velocities and positions are no longer detected when we analyze Sample2 and the "virialized sample". Thus, we suspect that the correlations found are not really due to cluster structure, but rather to the large-scale structure environment. On the other hand the direction of the velocity gradient coincides with that shown by the cluster elongation in the 2D analysis (see in the following). In all our three samples, the BCMI shows evidence of peculiarity according to

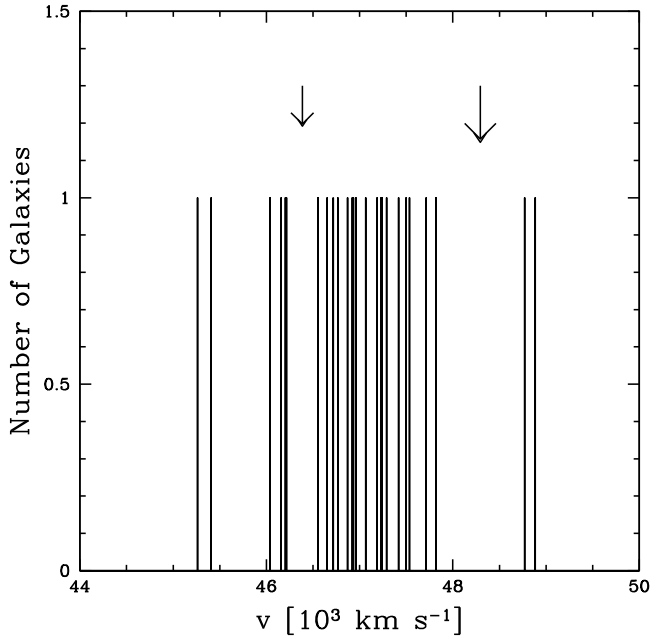

Fig. 19. A796: stripe density plot where the big (small) arrow indicates the position of the significant gap in the velocity distribution of the whole system (Sample2).

Table 6. A796: results of the kinematical analysis.

Sample	N_g	$\langle v \rangle$ km s^{-1}	σ_V km s^{-1}	R_{vir} Mpc	Mass($<R_{vir}$) 10^{14} $M_\odot$
Whole system	26	46 942 ± 140	698^{+216}_{-159}	1.57	$6.9^{+4.0}_{-3.0}$
Whole system Sample2	24	46 921 ± 120	571^{+134}_{-73}	1.29	$3.9^{+2.4}_{-2.2}$
Virialized subsample	14	46 796 ± 165	586^{+171}_{-148}	1.32	$4.6^{+2.4}_{-1.6}$

the Indicator test by Gebhardt & Beers (1991, at the >95% c.l.) with respect to the whole system.

Considering Sample2, we find a weighted gap which separates the velocity distribution in a low and a high velocity set (see Fig. 19). Very interestingly, the two most luminous galaxies BCMI and BCMInc lie in the low and high velocity sets, respectively. This is suggestive of a situation similar to that of A610, i.e., a possible merger between two subclusters.

5.2. 2D galaxy distribution

When applying the DEDICA method to the 2D distribution of A796 galaxy members we find that the cluster is elongated along the SE-NW direction. To check this finding we recover the photometric catalog extracted from the SDSS DR5. Figure 20 shows the result of the DEDICA method applied to the $r' \leq 20$ likely members selected on the basis of their colors – i.e., only galaxies lying within 0.08 mag from $r'-i' = 0.46$ and $i'-z' = 0.33$ colors. We confirm the cluster elongation finding two minor peaks in the SE and NW directions. Similar results are found for different magnitude cuts $r' \leq 19$ and $r' \leq 21$.

6. Summary and conclusions

We present the results of a dynamical analysis of the three poor, low X-ray luminous clusters A610, A725, and A796 containing diffuse radio sources (relic, relic, and a possible halo, respectively). Our analysis is based on new redshift data for

Table 7. Properties of galaxy clusters.

Cluster	N	N_m	$N_{m,vir}$	α δ J2000	z	σ_V km s^{-1}	Mass($<R_{vir}$) 10^{14} $M_\odot$
A610	165	57	22	075917.10 + 270916.1	0.098	426–496	1.8–2.3
A725	51	36	27	090109.99 + 623720.0	0.092	~534	~3.2
A796	99	26	14	092757.55 + 602633.7	0.157	571–698	3.9–6.9

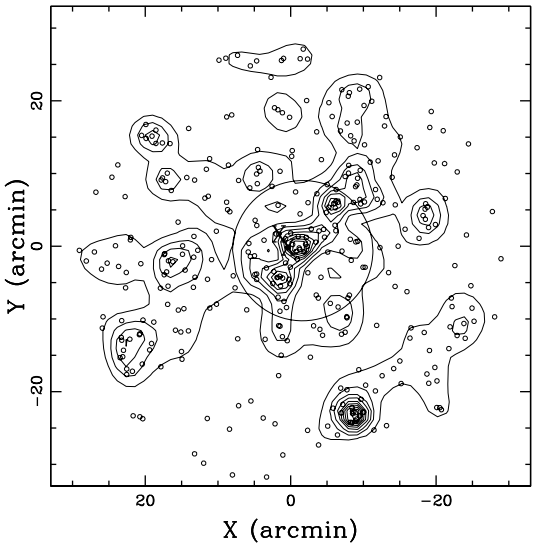

Fig. 20. A796: spatial distribution on the sky and relative isodensity contour map of the 349 likely cluster members (according to the two colors selection) with $r' \leq 20$, obtained with the DEDICA method. The circle indicates the likely virialized region. The crosses indicate the two most luminous galaxies BCMI and BCMInc.

158 galaxies obtained at the WHT and additional SDSS DR5 data for A610 and A796. We also use new photometric data obtained at the INT for A725.

We select 57, 36 and 26 cluster members for A610, A725 and A796, respectively. Out of these galaxies 35, 36 and 17 were measured by the WHT.

The low values we compute for the global LOS velocity dispersion of galaxies (σ_V = 420–700 km s^{-1}) confirm that these clusters are low-mass clusters. Table 7 summarizes the main cluster properties as recovered in this study. Using the $\sigma_V - T_X$ relation by Girardi et al. (1998) the range of expected X-ray temperature of the intracluster gas is T_X = 2–3 keV. The study of these three clusters indicates that the phenomenon of diffuse radio sources is not limited to massive clusters only.

We also discuss the dynamical status and the possible connection with the diffuse sources of each individual cluster. Regarding the two clusters hosting a radio relic, A610 and A725, the former is better sampled and can be analyzed in greater detail. A610 shows a lot of evidence of substructure: the non-Gaussianity of the velocity distribution, the correlation between galaxy velocities and positions and the peculiarity of the BCMI in the velocity space. A610 seems formed by two structures separated by ~700 km s^{-1} in the cluster rest-frame, having comparable $\sigma_V \sim 200$ km s^{-1} and likely causing a velocity gradient. Moreover, the BCMI velocity is very close to the mean velocity of the higher velocity structure. A third small, low velocity group hosts the BCMII. The analysis of the 2D galaxy distribution shows a bimodal distribution in the core – elongated in the SE-NW direction and likely associated to BCMI and BCMII groups – as well as the presence of an eastern group just outside the virialized region. In this chaotic scenario, it is not easy to unveil the event responsible for the relic. One possibility is that the relic be associated to the likely merger between the two structures corresponding to BCMI and BCMII. In this case it would be somewhat perpendicular to the axis connecting the two merging structures (see Fig. 1) in agreement with being originated by shock waves connected to the ongoing merger (e.g., Ensslin & Brüggen 2002). Another possibility is that the relic be related to the merger between the two main velocity structures forming the cluster (see Fig. 4). This would be more likely from the energetic point of view since this merger involves structures of 1:1 mass ratio. In conclusion, A610 represents another case of a radio cluster formed by two merging subclusters, like, e.g., A115 (Barrena et al. 2007b); A2744 (Boschin et al. 2006); and A773 (Barrena et al. 2007a), but at much smaller scales (global $\sigma_V \sim 500$ km s^{-1} vs. $\sigma_V > 1000$ km s^{-1}). As a further support to the merging scenario, we notice that the BCMI of A610 is also a bright radio source with a WAT structure. This is very interesting because WATs are only found in galaxy clusters and are excellent probes of the gas-dynamical processes occuring during a cluster merger (e.g., Gómez et al. 1997).

As for A725, it shows some evidence of non-Gaussianity in the velocity distribution, the peculiarity of the BCMI in the velocity space, and an elongated cluster shape in the NE-SW direction. This direction is the same one indicated by the radio relic since it is an arc of diffuse emission to the NE of the radio galaxy associated with the BCMI (Kempner & Sarazin 2001, see Fig. 11).

A796 possibly hosts a radio halo (to be confirmed) according to WENSS data (Kempner & Sarazin 2001). It shows the peculiarity of the BCMI in the velocity space, possible spatial/velocity substructure and the presence of two minor clumps along the SE-NW direction.

For A725 and A796 the number of cluster members (~30) is enough for the estimate of σ_V, but too small for the analysis of substructure. Thus, a definitive conclusion will require more data.

Acknowledgements. We would like to thank Luigina Feretti for many enlightening discussions and for the VLA radio image of A610 she kindly provided us. We thank the anonymous referee for useful comments and suggestions.
This publication is based on observations made on the island of La Palma with the William Herschel Telescope (WHT) and with the Isaac Newton Telescope (INT), operated by the Isaac Newton Group (ING), in the Spanish Observatory of the Roque de Los Muchachos of the Instituto de Astrofisica de Canarias.
This research has made use of the NASA/IPAC Extragalactic Database (NED), which is operated by the Jet Propulsion Laboratory, California Institute of Technology, under contract with the National Aeronautics and Space Administration.
This research has made use of the galaxy catalog of the Sloan Digital Sky Survey (SDSS). Funding for the SDSS has been provided by the Alfred P. Sloan Foundation, the Participating Institutions, the National Aeronautics and Space Administration, the National Science Foundation, the U.S. Department of Energy, the Japanese Monbukagakusho, and the Max Planck Society. The SDSS Web site is http://www.sdss.org/.
The SDSS is managed by the Astrophysical Research Consortium for the Participating Institutions. The Participating Institutions are the American Museum of Natural History, Astrophysical Institute Potsdam, University of Basel, University of Cambridge, Case Western Reserve University, University

of Chicago, Drexel University, Fermilab, the Institute for Advanced Study, the Japan Participation Group, Johns Hopkins University, the Joint Institute for Nuclear Astrophysics, the Kavli Institute for Particle Astrophysics and Cosmology, the Korean Scientist Group, the Chinese Academy of Sciences (LAMOST), Los Alamos National Laboratory, the Max-Planck-Institute for Astronomy (MPIA), the Max-Planck-Institute for Astrophysics (MPA), New Mexico State University, Ohio State University, University of Pittsburgh, University of Portsmouth, Princeton University, the United States Naval Observatory, and the University of Washington.

This work was partially supported by a grant from the Istituto Nazionale di Astrofisica (INAF, grant PRIN-INAF2006 CRA ref number 1.06.09.06).

References

Abell, G. O., Corwin, H. G. Jr., & Olowin, R. P. 1989, ApJS, 70, 1
Ashman, K. M., Bird, C. M., & Zepf, S. E. 1994, AJ, 108, 2348
Bardelli, S., Zucca, E., Vettolani, G., et al. 1994, MNRAS, 267, 665
Barrena, R., Biviano, A., Ramella, M., Falco, E. E., & Seitz, S. 2002, A&A, 386, 816
Barrena, R., Boschin, W., Girardi, M., & Spolaor, M. 2007a, A&A, 467, 37
Barrena, R., Boschin, W., Girardi, M., & Spolaor, M. 2007b, A&A, 469, 861
Beers, T. C., Flynn, K., & Gebhardt, K. 1990, AJ, 100, 32
Beers, T. C., Forman, W., Huchra, J. P., Jones, C., & Gebhardt, K. 1991, AJ, 102, 1581
Bertin, E., & Arnouts, S. 1996, A&AS, 117, 393
Bird, C. M. 1994, ApJ, 422, 480
Bird, C. M., & Beers, T. C. 1993, AJ, 105, 1596
Böhringer, H., & Schuecker, P. 2002, in Merging Processes in Galaxy Clusters, ed. L. Feretti, I. M. Gioia, & G. Giovannini, Observational signatures and statistics of galaxy cluster mergers (The Netherlands: Kluwer Ac. Pub.)
Böhringer, H., Voges, W., Huchra, J. P., et al. 2002, ApJS, 129, 435
Boschin, W., Girardi, M., Barrena, R., et al. 2004, A&A, 416, 839
Boschin, W., Girardi, M., Spolaor, M., & Barrena, R. 2006, A&A, 449, 461
Buote, D. A. 2001, ApJ, 553, L15
Buote, D. A. 2002, in Merging Processes in Galaxy Clusters, ed. L. Feretti, I. M. Gioia, & G. Giovannini, Optical Analysis of Cluster Mergers (The Netherlands: Kluwer Ac. Pub.)
Burns, J. O., Roettiger, K., Ledlow, M., & Klypin, A. 1994, ApJ, 427, L87
Burstein, D., & Heiles, C. 1982, AJ, 87, 1165
Carlberg, R. G., Yee, H. K. C., & Ellingson, E. 1997, ApJ, 478, 462
Cassano, R., Brunetti G., & Setti, G. 2006, MNRAS, 369, 1577
Cousins, A. W. J. 1976, MemRAS, 81, 25
Danese, L., De Zotti, C., & di Tullio, G. 1980, A&A, 82, 322
den Hartog, R., & Katgert, P. 1996, MNRAS, 279, 349
Ellingson, E., & Yee, H. K. C. 1994, ApJS, 92, 33
Ensslin, T. A., & Brüggen, M. 2002, MNRAS, 331, 1011
Fadda, D., Girardi, M., Giuricin, G., Mardirossian, F., & Mezzetti, M. 1996, ApJ, 473, 670
Feretti, L. 1999, MPE Rep., 271
Feretti, L. 2002, The Universe at Low Radio Frequencies, held 30 Nov.−4 Dec. 1999, Pune, India, ed. A. Pramesh Rao, G. Swarup, & Gopal-Krishna, Proc. IAU Symp., 199, 133
Feretti, L. 2005, X-Ray and Radio Connections, Published electronically by NRAO, http://www.aoc.nrao.edu/events/xraydio, Held 3−6 February 2004 in Santa Fe, New Mexico, USA, ed. L. O. Sjouwerman, & K. K. Dyer
Gebhardt, K., & Beers, T. C. 1991, ApJ, 383, 72
Giovannini, G., & Feretti, L. 2000, New Astron., 5, 335
Giovannini, G., & Feretti, L. 2002, in Merging Processes in Galaxy Clusters, ed. L. Feretti, I. M. Gioia, & G. Giovannini, Diffuse Radio Sources and Cluster Mergers (The Netherlands: Kluwer Ac. Pub.)
Giovannini, G., Feretti, L., Venturi T., Kim, K.-T., & Kronberg, P. P. 1993, ApJ, 406, 399
Giovannini, G., Tordi, M., & Feretti, L. 1999, New Astron., 4, 141
Girardi, M., & Biviano, A. 2002, in Merging Processes in Galaxy Clusters, ed. L. Feretti, I. M. Gioia, & G. Giovannini, Analysis of Cluster Mergers (The Netherlands: Kluwer Ac. Pub.)
Girardi, M., & Mezzetti, M. 2001, ApJ, 548, 79
Girardi, M., Fadda, D., Giuricin, G., et al. 1996, ApJ, 457, 61
Girardi, M., Giuricin, G., Mardirossian, F., Mezzetti, M., & Boschin, W. 1998, ApJ, 505, 74
Girardi, M., Boschin, W., & Barrena, R. 2006, A&A, 455, 45
Gómez, P. L., Pinkney, J., Burns, J. O., et al. 1997, ApJ, 474, 580
Govoni, F., Ensslin, T. A., Feretti, L., & Giovannini, G. 2001a, A&A, 369, 441
Govoni, F., Feretti, L., Giovannini, G., et al. 2001b, A&A, 376, 803
Goto, T., Sekiguchi, M., Nichol, R. C., et al. 2002, AJ, 123, 1807
Gullixson, C. A. 1992, in Astronomical CCD Observing and Reduction Techniques, ed. S. B. Howell, ASP Conf. Ser., 23, 130
Hanisch, R. J. 1982, A&A, 116, 137
Jetha, N. N., Hardcastle, M. J., & Sakelliou, I. 2006, MNRAS, 368, 609
Johnson, H. L., & Morgan, W. W. 1953, ApJ, 117, 313
Kempner, J. C., & Sarazin, C. L. 2001, ApJ, 548, 639
Kennicutt, R. C. 1992, ApJS, 79, 225
Kowalski, M. P., Ulmer, M. P., Cruddace, R. G., & Wood, K. S. 1984, ApJS, 56, 403
Limber, D. N., & Mathews, W. G. 1960, ApJ, 132, 286
López-Cruz, O., Barkhouse, W. A., & Yee, H. K. C. 2004, ApJ, 614, 679
Malumuth, E. M., Kriss, G. A., Dixon, W. Van Dyke, Ferguson, H. C., & Ritchie, C. 1992, AJ, 104, 495
Maurogordato, S., Cappi, A., Ferrari, C., et al. 2008, A&A, in press
Mercurio, A., Girardi, M., Boschin, W., Merluzzi, P., & Busarello, G. 2003, A&A, 397, 431
Owen, F. N., White, R. A., & Burns, J. O. 1992, ApJS, 80, 501
Owen, F. N., White, R. A., & Jingping, G. 1993, ApJS, 87, 135
Owen, F. N., Ledlow, M. J., & Keel, W. C. 1995, AJ, 109, 14
Pisani, A. 1993, MNRAS, 265, 706
Pisani, A. 1996, MNRAS, 278, 697
Poggianti, B. M. 1997, A&AS, 122, 399
Press, W. H., Teukolsky, S. A., Vetterling, W. T., & Flannery, B. P. 1992, in Numerical Recipes, 2nd Ed. (Cambridge University Press)
Quintana, H., Carrasco, E. R., & Reisenegger, A. 2000, AJ, 120, 511
Roettiger, K., Loken, C., & Burns, J. O. 1997, ApJS, 109, 307
Röttgering, H., Snellen, I., Miley, G., et al. 1994, ApJ, 436, 654
Sarazin, C. L. 2002, in Merging Processes in Galaxy Clusters, The Physics of Cluster Mergers, ed. L. Feretti, I. M. Gioia, & G. Giovannini (The Netherlands: Kluwer Ac. Pub.)
Schuecker, P., Böhringer, H., Reiprich, T. H., & Feretti, L. 2001, A&A, 378, 408
Shapiro, S. S., & Wilk, M. B. 1965, Biometrika, 52, 591
Struble, M. F., & Rood, H. J. 1982, AJ, 87, 7
Struble, M. F., & Rood, H. J. 1984, AJ, 89, 1487
The, L. S., & White, S. D. M. 1986, AJ, 92, 1248
Tonry, J., & Davis, M. 1979, AJ, 84, 1511
Tribble, P. 1993, MNRAS, 263, 31
Valentijn, E. A. 1979, ApJS, 38, 319
Wainer, H., & Schacht, S. 1978, Psychometrika, 43, 203

Table 1. Velocity catalog of 165 spectroscopically measured galaxies in the field of A610. In Col. 1, IDs in italics indicate non-cluster galaxies. IDs 91 and 98 (in boldface) are, respectively, the first and the second brightest galaxies of the cluster. Asterisks in Col. 1 highlight QSOs in the SDSS catalog.

ID	α, δ (J2000)	r'	v (km s^{-1})	Δv	Source
1	7 57 04.15, +27 13 13.3	17.65	29 052	16	S
2	7 57 08.66, +27 09 46.4	17.51	19 274	28	S
3	7 57 09.21, +27 07 06.9	16.71	34 657	50	S
4	7 57 12.09, +27 03 23.8	16.32	29 776	46	S
5	7 57 18.01, +27 07 51.1	16.92	19 291	44	S
6	7 57 18.16, +27 04 57.8	15.72	19 913	45	S
7	7 57 22.92, +27 00 08.5	15.93	19 633	43	S
*8**	7 57 24.02, +26 58 46.9	18.94	720 155	395	S
9	7 57 25.29, +27 23 21.9	18.37	30 870	40	S
10	7 57 26.27, +27 20 01.3	17.22	37 076	39	S
11	7 57 26.55, +27 05 00.3	16.58	29 492	41	S
12	7 57 32.19, +27 14 03.1	17.36	20 638	23	S
13	7 57 32.84, +27 17 51.3	16.40	37 190	44	S
14	7 57 38.68, +27 22 29.0	18.42	69 538	43	S
15	7 57 39.03, +26 50 42.6	16.38	8076	16	S
16	7 57 40.71, +26 57 28.9	17.70	29 271	18	S
17	7 57 43.25, +27 08 04.3	17.52	36 975	46	S
18	7 57 43.57, +27 19 38.2	16.15	37 018	46	S
19	7 57 44.76, +26 55 06.3	19.09	135 715	64	S
20	7 57 47.25, +27 18 42.7	17.38	42 430	46	S
21	7 57 49.87, +27 01 45.5	16.95	21 660	15	S
*22**	7 57 50.40, +26 55 14.7	18.69	689 658	435	S
23	7 57 50.44, +27 07 22.9	17.60	21 562	36	W + S
24	7 57 51.13, +27 09 41.8	17.71	13 929	12	W + S
25	7 57 51.74, +27 29 33.5	17.23	62 598	49	S
26	7 57 52.54, +26 59 31.1	17.40	29 769	40	W + S
27	7 57 58.64, +27 10 17.0	17.05	21 681	19	W + S
*28**	7 57 58.93, +27 31 02.7	19.00	431 857	470	S
29	7 57 59.88, +27 04 09.2	17.38	29 630	25	S
30	7 58 00.36, +27 08 41.9	16.93	28 778	37	S
31	7 58 00.96, +27 05 53.8	16.12	28 890	30	W + S
*32**	7 58 04.51, +27 07 18.2	19.12	448 615	286	S
33	7 58 05.84, +27 16 56.9	16.58	28 919	30	W + S
34	7 58 06.68, +27 24 40.2	16.93	7769	30	S
35	7 58 08.69, +27 08 15.5	17.59	28 924	33	W + S
36	7 58 10.17, +27 21 04.7	16.57	6841	45	S
37	7 58 11.69, +27 11 28.6	17.46	29 287	31	W + S
38	7 58 13.82, +27 15 12.7	17.54	23 099	14	S
39	7 58 16.58, +27 03 43.9	18.40	43 608	101	W
40	7 58 16.66, +27 10 29.6	14.51	13 818	39	W + S
41	7 58 17.86, +27 03 23.9	14.68	6386	24	W + S
*42**	7 58 18.29, +27 05 16.5	19.89	740 173	237	S
43	7 58 22.66, +26 41 20.6	17.48	68 989	38	S
44	7 58 26.22, +27 09 41.5	15.74	14 116	17	W + S
45	7 58 26.37, +27 00 37.5	16.63	30 012	39	S
46	7 58 28.45, +26 40 53.9	17.67	24 891	42	S
47	7 58 28.97, +26 39 49.6	16.77	70 367	52	S
48	7 58 29.80, +27 18 23.5	17.53	29 199	33	W + S
49	7 58 30.83, +27 13 33.5	17.44	29 486	33	W + S
50	7 58 33.27, +27 02 18.1	16.41	29 734	29	W + S
*51**	7 58 33.99, +27 11 51.4	18.89	69 649	261	S
52	7 58 36.35, +27 18 42.0	17.75	22 657	6	W + S
53	7 58 36.45, +27 11 36.8	18.04	29 153	74	W
54	7 58 39.62, +26 51 47.7	17.77	36 780	29	S
55	7 58 40.38, +26 56 39.3	16.79	36 893	21	W + S
56	7 58 41.26, +26 58 14.6	17.12	22 338	26	W + S
57	7 58 42.45, +27 16 56.0	17.45	28 757	21	W + S
58	7 58 46.68, +27 34 51.9	15.90	22 936	51	S
59	7 58 46.99, +27 05 15.6	17.15	29 621	52	S
60	7 58 47.87, +26 47 35.8	16.96	22 240	17	S
61	7 58 47.96, +27 17 06.0	16.33	28 705	31	W + S
62	7 58 49.67, +27 27 55.9	17.42	29 039	35	S
63	7 58 52.31, +27 24 01.6	18.23	20 449	120	W
64	7 58 52.99, +27 12 51.2	17.62	29 272	30	W + S
65	7 58 54.80, +27 11 28.5	17.63	28 444	39	S
66	7 58 56.31, +27 33 24.7	16.44	22 937	56	S
67	7 58 56.53, +27 03 17.2	17.39	13 626	12	S
68	7 58 58.20, +27 09 37.1	15.84	22 629	31	W + S
69	7 58 59.33, +27 12 56.8	16.68	28 846	39	W + S
70	7 59 00.21, +27 35 33.9	16.92	14 101	29	S
71	7 59 00.70, +27 33 52.8	17.01	37 403	50	S
72	7 59 01.04, +27 07 12.1	17.30	29 007	29	W + S
73	7 59 01.10, +27 09 43.3	16.52	25 836	26	W
74	7 59 01.28, +27 06 11.8	17.36	29 190	35	S
75	7 59 03.63, +26 53 09.7	17.05	22 372	28	W + S
76	7 59 04.34, +27 08 55.4	16.86	28 833	40	S
77	7 59 04.34, +27 13 25.6	16.83	29 178	38	W + S
78	7 59 05.16, +27 27 34.3	15.32	6741	54	S
79	7 59 05.81, +27 06 29.8	16.77	29 277	35	W + S
80	7 59 06.22, +27 15 39.4	16.54	22 300	78	W
81	7 59 06.80, +26 50 54.4	18.37	99 637	46	S
82	7 59 07.49, +27 18 12.0	17.41	24 710	15	W + S
83	7 59 08.52, +27 11 27.1	17.41	29 123	15	W + S
84	7 59 09.00, +27 33 15.6	17.44	23 184	13	S
85	7 59 10.27, +26 49 07.1	16.08	20 469	44	S
86	7 59 11.37, +27 10 50.7	17.31	30 233	43	W
87	7 59 12.89, +27 06 16.0	16.96	30 172	53	W
88	7 59 13.65, +27 05 41.0	16.14	29 016	40	W
89	7 59 13.80, +26 38 22.8	17.56	6473	28	S
90	7 59 16.02, +27 08 57.7	17.60	29 242	23	S
91	7 59 17.10, +27 09 16.1	15.19	29 808	103	W
92	7 59 17.87, +27 04 40.3	13.72	6808	50	S
93	7 59 18.74, +27 07 10.2	17.42	27 598	39	S
94	7 59 20.05, +27 09 50.4	16.38	29 693	36	W + S
95	7 59 24.05, +27 08 49.5	16.24	29 901	38	W
96	7 59 24.24, +26 57 32.4	17.95	6299	56	W
97	7 59 24.36, +27 17 55.4	17.52	22 809	14	W + S
98	7 59 25.00, +27 07 48.9	15.72	27 901	42	W + S
99	7 59 27.79, +27 07 03.7	17.07	28 709	26	W + S
100	7 59 27.83, +27 05 45.4	15.97	20 444	30	W + S
101	7 59 28.52, +26 53 22.6	14.24	7924	23	S
102	7 59 29.71, +27 01 35.2	12.60	6654	59	S
103	7 59 32.18, +26 38 18.0	15.87	22 442	41	S
104	7 59 32.83, +26 55 08.6	17.98	45 163	79	W
105	7 59 33.50, +26 43 50.3	16.23	14 062	16	S
106	7 59 37.79, +26 57 29.6	17.43	29 709	26	W + S
107	7 59 38.39, +27 33 25.7	17.17	24 596	15	S
108	7 59 40.16, +27 05 14.1	17.22	14 234	20	W + S
109	7 59 40.18, +27 30 30.9	16.50	23 160	41	S
110	7 59 40.90, +27 35 45.2	16.54	22 861	43	S
111	7 59 41.72, +27 00 12.6	15.43	6642	27	W + S
112	7 59 42.16, +27 19 17.0	18.36	27 799	134	W
113	7 59 43.49, +27 10 10.9	17.13	29 631	43	S
114	7 59 44.15, +27 23 13.4	16.94	47 209	40	S
115	7 59 46.49, +26 38 19.2	17.79	8121	17	S
116	7 59 47.17, +27 31 24.3	17.58	31 213	35	S
117	7 59 48.38, +27 11 37.1	18.30	87 323	34	S
118	7 59 49.80, +27 09 37.1	17.90	20 839	105	W
119	7 59 51.25, +26 50 42.3	17.12	49 160	15	W + S
120	7 59 53.83, +26 47 20.5	15.12	14 223	19	S
121	7 59 54.14, +27 01 23.5	17.77	28 725	34	S
122	7 59 54.42, +27 08 54.7	17.59	30 176	34	S
123	7 59 55.14, +26 50 35.2	17.45	49 281	60	W
124	7 59 55.22, +27 07 47.8	17.31	13 978	13	S
125	7 59 57.75, +26 53 14.7	17.57	29 480	38	S
126	7 59 59.13, +27 09 02.5	17.52	20 722	84	W

Table 1. continued.

Table 1. continued.

ID	α, δ (J2000)	r'	v (km s^{-1})	Δv	Source
127	7 59 59.84, +26 57 39.0	18.53	29 882	60	W
128	8 00 00.02, +27 33 27.0	16.35	31 067	45	S
129	8 00 00.14, +27 09 00.1	17.80	20 572	12	S
130	8 00 01.06, +26 39 57.1	14.11	8129	46	S
131	8 00 01.92, +27 06 52.4	15.95	12 793	15	W + S
*132**	8 00 02.92, +27 17 27.4	19.96	567 201	830	S
*133**	8 00 06.60, +26 50 54.7	18.95	700 666	404	S
134	8 00 06.98, +27 09 38.7	17.37	29 521	33	W + S
135	8 00 07.36, +27 08 19.8	16.60	29 108	40	W + S
136	8 00 07.96, +26 42 24.4	15.95	14 162	43	S
137	8 00 11.64, +27 14 22.6	16.99	29 012	29	W + S
138	8 00 11.79, +27 32 30.0	16.28	30 944	36	S
139	8 00 14.08, +27 18 35.4	17.57	14 802	15	S
140	8 00 14.30, +26 41 52.8	14.87	8407	16	S
*141**	8 00 14.90, +27 20 36.2	19.31	1 135 030	131	S
142	8 00 15.38, +27 12 50.1	17.78	29 462	65	W
143	8 00 19.77, +26 42 05.2	13.91	8335	26	S
144	8 00 20.77, +27 26 24.9	17.63	58 497	54	S
145	8 00 21.25, +27 09 09.8	17.46	29 279	28	W + S
146	8 00 22.22, +27 07 52.5	16.27	29 125	31	W + S
147	8 00 22.54, +27 03 08.1	18.22	28 402	91	W
148	8 00 25.93, +27 06 59.1	17.06	28 862	34	S
149	8 00 30.46, +27 02 13.7	16.58	23 138	19	S
150	8 00 31.67, +26 45 11.7	16.06	14 240	16	S
151	8 00 39.10, +27 27 06.5	17.76	11 190	17	S
152	8 00 40.35, +26 59 15.7	17.21	28 800	36	S
153	8 00 41.73, +27 28 22.3	16.11	14 135	40	S
154	8 00 42.93, +27 13 47.7	16.90	29 235	20	S
155	8 00 47.14, +27 09 01.0	17.11	23 134	38	S
156	8 00 48.75, +26 59 10.4	16.06	6849	40	S
157	8 00 53.09, +27 13 37.6	16.58	13 917	44	S
*158**	8 00 55.32, +27 16 52.7	18.84	532 494	447	S
159	8 00 57.27, +27 12 28.0	17.08	49 350	37	S
*160**	8 00 57.36, +26 57 24.1	18.95	567 456	306	S
161	8 01 00.32, +27 10 46.8	17.00	14 287	46	S
162	8 01 14.34, +27 11 12.4	17.14	14 226	13	S
163	8 01 18.51, +27 12 45.5	14.47	14 101	47	S
164	8 01 22.04, +27 12 05.6	16.21	14 511	45	S
165	8 01 28.93, +27 04 32.3	16.05	30 157	41	S

Table 4. Velocity catalog of 51 spectroscopically measured galaxies in the field of A725. In Col. 1, IDs in italics indicate non–cluster galaxies. ID 24 (in boldface) is BCMI (see text).

ID	α, δ (J2000)	R	B	v (km s^{-1})	Δv
1	08 58 55.32, +62 44 53.4	–	–	8079	68
2	08 58 58.09, +62 36 23.5	16.18	18.35	26 850	39
3	08 59 06.88, +62 34 20.7	17.73	19.82	27 692	63
4	08 59 17.09, +62 33 21.3	16.43	18.07	27 339	52
5	08 59 32.75, +62 20 45.9	16.88	18.17	27 389	68
6	08 59 36.97, +62 20 46.3	–	–	27 473	82
7	08 59 41.35, +62 39 16.4	16.53	18.50	49 663	95
8	08 59 47.36, +62 37 58.6	17.68	19.14	28 261	70
9	08 59 55.76, +62 35 55.6	17.45	19.27	28 561	90
10	09 00 22.25, +62 43 29.2	16.61	18.61	26 269	47
11	09 00 22.42, +62 19 07.5	–	–	13 495	49
12	09 00 25.98, +62 37 45.8	16.52	18.69	27 461	49
13	09 00 32.55, +62 42 00.8	16.81	18.90	27 293	60
14	09 00 35.62, +62 43 59.4	16.83	18.51	27 457	79
15	09 00 37.96, +62 50 33.7	17.37	19.18	50 005	37
16	09 00 38.09, +62 38 05.7	16.67	18.66	27 620	105
17	09 00 42.36, +62 34 49.2	16.86	19.04	27 414	117
18	09 00 48.50, +62 35 55.0	16.79	18.29	28 471	53
19	09 00 55.68, +62 37 49.5	15.57	17.64	29 360	48
20	09 00 55.72, +62 30 06.6	18.25	19.84	53 737	52
21	09 00 57.04, +62 32 57.8	15.91	18.12	27 235	24
22	09 00 58.85, +62 38 31.9	16.09	16.87	27 739	49
23	09 01 03.65, +62 36 52.9	15.62	17.67	28 023	45
24	09 01 09.99, +62 37 20.0	15.12	16.41	27 104	48
25	09 01 11.08, +62 39 27.9	16.61	18.70	28 324	42
26	09 01 14.79, +62 36 10.6	15.44	17.59	27 449	22
27	09 01 34.70, +62 37 16.1	16.99	19.14	27 616	103
28	09 01 34.95, +62 33 32.7	17.56	18.63	25 973	23
29	09 01 35.40, +62 33 21.1	17.75	19.12	30 626	147
30	09 01 36.99, +62 38 38.3	15.79	17.80	27 716	43
31	09 01 40.93, +62 37 59.9	17.01	19.05	27 942	83
32	09 01 49.97, +62 42 33.6	16.37	18.37	27 018	60
33	09 01 52.04, +62 34 42.9	18.15	19.20	27 537	155
34	09 01 52.15, +62 34 12.3	16.08	18.25	26 873	75
35	09 02 06.50, +62 54 40.7	–	–	90 943	101
36	09 02 07.78, +62 40 40.7	16.27	18.24	26 846	84
37	09 02 09.60, +62 19 30.4	–	–	11 134	122
38	09 02 09.98, +62 45 01.1	17.70	19.65	27 530	75
39	09 02 15.21, +62 40 16.4	14.88	17.16	27 108	48
40	09 02 16.28, +62 32 25.7	17.66	19.65	53 311	57
41	09 02 19.33, +62 38 58.1	17.40	19.18	27 659	68
42	09 02 19.51, +62 48 14.1	17.66	19.16	28 592	95
43	09 02 19.58, +62 22 16.3	17.46	19.74	48 789	91
44	09 02 20.67, +62 45 44.8	17.72	19.58	52 418	68
45	09 02 29.76, +62 28 31.3	16.77	18.75	26 878	130
46	09 02 57.75, +62 22 00.1	–	–	62 471	71
47	09 02 58.11, +62 48 45.0	–	–	27 632	79
48	09 02 58.30, +62 38 56.7	–	–	22 394	47
49	09 03 01.38, +62 39 31.4	–	–	22 240	103
50	09 03 06.77, +62 49 39.6	–	–	27 267	73
51	09 03 13.73, +62 38 32.5	–	–	50 197	83

Table 5. Velocity catalog of 99 spectroscopically measured galaxies in the field of A796. In Col. 1, IDs in italics indicate non-cluster galaxies. IDs 54 and 56 (in boldface) are the brightest cluster members. Asterisks in Col. 1 highlight QSOs in the SDSS catalog.

ID	α, δ (J2000) $09^h, +60°$	r'	v (km s^{-1})	Δv	Source
*1**	24 03.66, 22 43.1	18.39	289 995	375	S
*2**	24 24.87, 14 59.2	18.61	644 626	405	S
3	24 44.13, 13 53.3	17.66	68 395	54	S
4	24 45.38, 15 55.2	17.52	59 869	54	S
5	25 07.51, 04 52.1	19.27	134 817	84	S
*6**	25 13.33, 10 39.2	17.68	254 929	498	S
7	25 26.14, 31 41.4	17.49	77 745	57	S
8	25 36.67, 22 35.7	17.38	79 529	48	S
9	25 39.80, 07 29.9	17.23	47 241	51	S
10	25 50.79, 17 13.2	19.38	47 187	78	W
*11**	25 59.93, 26 48.5	18.17	191 738	492	S
12	26 03.83, 36 02.6	17.19	46 654	45	S
*13**	26 12.49, 21 02.7	19.27	553 642	525	S
*14**	26 14.75, 25 58.4	19.39	670 723	462	S
15	26 19.73, 30 15.7	18.12	77 784	45	S
16	26 20.66, 33 01.5	16.91	33 780	38	W + S
17	26 23.36, 42 20.1	17.32	30 615	18	S
18	26 25.94, 05 09.6	17.63	46 216	30	S
19	26 30.12, 48 30.3	17.00	43 218	42	S
20	26 30.33, 28 52.9	17.96	90 115	45	S
21	26 34.66, 23 39.8	17.93	39 946	57	W
22	26 37.08, 23 39.4	17.73	39 701	45	S
23	26 39.52, 37 01.0	16.97	21 478	70	W + S
24	26 44.25, 06 50.7	17.69	75 955	42	S
25	26 46.11, 03 39.7	17.21	47 418	48	S
26	26 46.15, 31 28.8	18.41	90 825	42	S
27	26 49.47, 27 24.2	18.22	45 262	56	W
28	26 49.88, 02 17.2	17.70	47 499	45	S
29	26 50.12, 24 36.7	17.60	39 648	42	S
30	26 51.06, 12 04.3	19.00	10 952	139	W
*31**	26 53.67, 22 17.4	20.17	455 885	468	S
32	26 53.98, 19 27.0	17.91	47 066	69	W
33	26 55.38, 06 49.3	18.91	53 621	64	W
*34**	26 56.95, 25 04.3	19.14	886 148	13 317	S
35	26 59.88, 48 05.4	15.39	30 681	45	S
36	27 01.69, 03 37.3	17.67	53 360	45	S
37	27 07.68, 31 50.7	17.61	46 872	75	W
38	27 07.80, 32 27.3	17.26	43 198	37	W + S
39	27 14.41, 38 43.9	19.02	54 241	58	W
40	27 14.95, 22 49.6	18.48	30 743	48	W
41	27 16.64, 35 02.6	17.57	43 341	33	W + S
42	27 25.60, 22 16.2	16.46	30 522	29	W + S
43	27 29.10, 19 51.0	17.80	69 182	31	W
44	27 29.38, 27 07.8	17.72	46 717	34	W
45	27 34.31, 11 07.5	17.05	22 480	40	W + S
46	27 40.19, 27 47.2	17.58	46 767	31	W + S
47	27 40.83, 26 50.4	18.16	45 407	110	W
48	27 42.87, 40 24.9	18.65	33 263	109	W
49	27 44.28, 08 39.3	18.29	21 315	98	W
50	27 47.09, 31 00.9	17.87	46 921	43	W
51	27 52.10, 34 01.7	17.73	39 922	83	W
52	27 53.74, 24 20.3	16.52	1286	39	S
53	27 58.61, 26 17.7	17.29	46 961	122	W
54	28 00.65, 26 26.8	16.96	46 038	29	W + S
55	28 03.20, 24 15.7	18.72	47 229	43	W
56	28 10.75, 28 15.0	16.94	46 934	39	W + S
57	28 11.89, 45 19.8	16.94	39 600	42	S
58	28 12.80, 22 16.7	17.62	47 534	37	W + S
59	28 14.76, 02 07.5	17.59	30 048	39	S
60	28 19.76, 49 47.3	16.26	26 987	48	S
61	28 24.54, 14 19.4	16.97	22 797	20	W + S
62	28 24.54, 23 34.8	17.84	47 290	40	W

Table 5. continued.

ID	α, δ (J2000) $09^h, +60°$	r'	v (km s^{-1})	Δv	Source
63	28 27.29, 27 24.1	18.77	46 554	58	W
64	28 33.51, 18 45.6	18.79	35 964	66	W
*65**	28 37.98, 25 21.0	16.86	88 574	477	S
66	28 41.44, 05 16.6	18.40	48 770	64	W
67	28 44.90, 25 45.8	17.40	46 204	39	S
68	28 50.43, 48 40.9	18.30	88 076	48	S
69	28 55.52, 51 33.6	17.56	73 272	45	S
70	28 57.65, 52 49.4	17.09	35 864	45	S
71	28 59.48, 20 50.4	16.96	22 734	37	W + S
72	29 15.19, 14 56.9	19.36	47 819	62	W
*73**	29 18.14, 17 06.3	19.03	665 093	435	S
74	29 27.43, 18 03.4	17.16	35 941	35	W + S
75	29 29.47, 02 51.2	17.38	48 884	42	S
76	29 32.16, 37 09.1	17.13	35 963	38	W + S
77	29 35.13, 33 06.2	17.30	44 039	41	W + S
78	29 50.93, 14 54.6	16.92	47 715	45	S
79	29 55.21, 23 17.2	16.25	36 079	23	W + S
80	29 58.50, 12 04.6	18.39	80 522	62	W
81	29 59.36, 14 46.1	17.62	54 170	39	W + S
*82**	30 04.28, 39 30.0	18.43	233 694	345	S
83	30 06.44, 26 53.4	16.93	4086	3	S
84	30 09.12, 28 05.6	16.29	4072	21	W + S
85	30 14.03, 21 04.6	17.66	42 978	32	W + S
86	30 26.63, 26 48.8	18.72	11 766	100	W
87	30 30.62, 22 05.0	18.34	50 023	35	W
88	30 33.74, 12 17.6	17.56	46 159	42	S
89	30 45.28, 14 23.0	17.51	65 622	51	S
*90**	30 51.94, 23 01.1	19.49	1 111 330	240	S
91	30 55.40, 04 36.7	19.30	163 600	69	S
92	31 05.10, 16 19.5	17.14	42 900	42	S
93	31 05.32, 14 01.1	17.30	53 867	45	S
94	31 09.48, 14 59.9	15.69	7765	27	S
95	31 11.54, 37 44.5	17.53	33 835	33	S
96	31 13.88, 06 29.1	19.12	187 991	417	S
97	31 17.95, 36 03.2	16.46	44 219	45	S
98	31 25.83, 16 50.4	17.50	43 062	42	S
*99**	31 30.71, 11 06.3	19.00	436 147	687	S